Preprints (www.preprints.org) | NOT PEER-REVIEWED | Posted: 19 April 2022 doi:10.20944/preprints202204.0175.v1

Article

Error Related Brain Microstate Analysis during A Complex Surgical Motor Task

Pushpinder Walia [1], Yaoyu Fu [2], Jack Norfleet [3], Steven D. Schwaitzberg [4], Xavier Intes [5,6], Suvranu De [5,6], Lora Cavuoto [2] and Anirban Dutta [1,*]

1. Neuroengineering and Informatics for Rehabilitation Laboratory, Department of Biomedical Engineering, University at Buffalo, Buffalo, NY, USA; pwalia@buffalo.edu(P.W.)
2. Department of Industrial and Systems Engineering, University at Buffalo, Buffalo, NY, USA; yaoyufu@buffalo.edu(Y.F.); loracavu@buffalo.edu(L.C.)
3. U.S. Army Futures Command, Combat Capabilities Development Command Soldier Center STTC, Orlando, FL, USA; jack.e.norfleet.civ@mail.mil(J.N.)
4. University at Buffalo School of Medicine and Biomedical Sciences, Buffalo, NY, USA; schwaitz@buffalo.edu(S.D.S.)
5. Center for Modeling, Simulation and Imaging in Medicine, Rensselaer Polytechnic Institute, Troy, NY, USA; intesx@rpi.edu(X.I.); des@rpi.edu(S.D.)
6. Department of Biomedical Engineering, Rensselaer Polytechnic Institute, Troy, NY, USA

* Correspondence: author: anirband@buffalo.edu

Abstract: Fundamentals of Laparoscopic Surgery (FLS) is a training module designed to provide basic surgical skills. During skill training of the FLS "suturing and intracorporeal knot-tying" task – the most difficult among the five psychomotor FLS tasks, learning from errors is one of the basic principles of motor skill acquisition where appropriate contextual switching of the brain state on error is postulated. This study investigated changes in the brain state following an error event based on the fusion of simultaneously acquired functional near-infrared spectroscopy (fNIRS) and electroencephalography (EEG) signals. Here, human error processing is postulated to differentiate experts from novices based on the differences in the error-related chain of mental processes. Thirteen right-handed novice medical students and nine expert surgeons participated in this study. Error-related microstate analysis was performed using 32-channel EEG data at a high temporal resolution. Six microstate prototypes were identified from combined EEG data from experts and novices during the FLS task. Analysis of variance (ANOVA) found that the proportion of the total time spent in different microstates during the 10 sec error epoch was significantly affected by the skill level ($p<0.01$), microstate type ($p<0.01$), and the interaction between the skill level and the microstate type ($p<0.01$). Then, the EEG band power (1-40Hz) related to slower oxyhemoglobin (HbO) changes were found using regularized temporally embedded Canonical Correlation Analysis of the fNIRS-EEG signals. The HbO signal from the fNIRS channel overlying 'Frontal_Inf_Oper_L', 'Frontal_Mid_Orb_L', 'Postcentral_L', 'Temporal_Sup_L', 'Frontal_Mid_Orb_R' cortical areas from Automatic Anatomical Labelling showed significant ($p<0.05$) difference between experts and novices in the 10-sec error epoch. Here, the frontal/prefrontal cortical areas are postulated to be related to the perception and the activation of the primary somatosensory cortex at the postcentral cortical area is hypothesized to be related to the action underpinning perception-action coupling model for the error-related chain of mental processes. Therefore, our study highlighted the importance of error-related brain states from portable brain imaging when comparing complex surgical skill levels.

Keywords: error; motor learning; surgical skills; EEG; fNIRS; neurovascular coupling

1. Introduction

Laparoscopic surgery training following the Fundamentals of Laparoscopic Surgery (FLS) is a common education and training module designed for medical residents, fellows,

© 2022 by the author(s). Distributed under a Creative Commons CC BY license.

Preprints (www.preprints.org) | NOT PEER-REVIEWED | Posted: 19 April 2022 doi:10.20944/preprints202204.0175.v1

and the physician to provide them with a set of basic surgical skills necessary to successfully conduct laparoscopic surgery. The FLS training is a joint education program between the Society of American Gastrointestinal Endoscopic Surgeons and the American College of Surgeon to establish box trainers (physical simulators) in standard surgical training curricula (Birkmeyer et al., 2013). FLS certification in general surgery in the USA uses five psychomotor tasks with increasing task complexity: (i) pegboard transfers, (ii) pattern cutting, (iii) placement of a ligating loop, (iv) suturing with extracorporeal knot tying, and (v) suturing with intracorporal knot tying. It was introduced to systemize training and evaluation of cognitive and psychomotor skills required to perform minimally invasive surgery. FLS is being used to measure and document those skills for medical practitioners. Understanding the brain-behavior relationship during skill learning is necessary for informed training and assessment (Dehabadi et al., 2014).

The FLS "suturing and intracorporeal knot-tying" task is the most difficult among the five psychomotor tasks that surgeons must pass as part of the board certification process. Laparoscopic suturing is a bimanual task that requires coordination of both hands. This skill enables surgeons to provide a wide range of advanced surgical procedures (Allen et al., 2003); however, acquiring this skill needs protracted training. The behavior can be characterized as a coordinated spatio-temporal 3D movement based on 2D camera feedback with the interaction between the body and the environment within a restricted surgical volume. Here, the FLS "suturing and intracorporeal knot-tying" is a complex bimanual motor task requiring high precision, hand-eye coordination, depth perception in the 2D view, and tool control for optimal performance (Hannah et al., 2022). Given the motor noise in tool control, error in-depth perception in the 2D view, and environmental changes in the hand-eye coordination, the task performance requires superior perception-action coupling. Here, the surgeon needs to cope with the uncertainties with an excellent perceptual model of the feedback (i.e., perceptual memory) besides the executive memory of the actions.

The perception, action, outcome, and prediction of the perception-action cycle occur iteratively in a cyclic manner throughout the task for the orderly descent from prefrontal to premotor to motor cortex in Fuster's perception-action processing stages (Fuster, 2004). Here, the information flow from perception to action and action to perception involves a cyclic flow of information between the environment and the organism, which can be used to learn a sensory-guided sequence of goal-directed actions. However, sensory feedback is noisy and delayed. At the same time, the motor actions are variable, so the solution to these challenges is an adaptive internal model of the body and the environment that needs to be continuously learned from sensory prediction errors (Shadmehr et al., 2010). Then, during sensorimotor adaptation, error correction carries an implicit cost for the brain (Sedaghat-Nejad and Shadmehr, 2021), so acquiring expert performance requires deliberate practice (Ericsson, 2006) despite the cost. Indeed, automaticity can be achieved despite residual error when there is an increased speed of action selection at the cost of cognitive flexibility (Poldrack et al., 2005; Toner et al., 2015). Therefore, it is postulated that cognitively controlled and automated processes must operate in parallel (Toner and Moran, 2021) during the task.

Learning from errors due to perturbations in performance is one of the basic principles of motor skill acquisition (Diedrichsen et al., 2010), where appropriate contextual switching of brain state on error is postulated to be necessary under perception-action coupling (Benozzo et al., 2021). Here, the changing brain states can be captured by microstates (Michel and Koenig, 2018) that are global patterns of quasi-stable (60–120 ms) scalp potential topographies of the large-scale brain networks (Lehmann et al., 1987). For example, post-error slowing (PES) and post-error improvement of accuracy (PIA) following error commission (Perri et al., 2016) during the acquisition of expert performance can be considered as appropriate contextual switching of the brain state. The scalp topographies of post-correct and post-error trials reflect the role of prefrontal and premotor areas in post-error adjustments (Perri et al., 2016). Here, the medial

Preprints (www.preprints.org) | NOT PEER-REVIEWED | Posted: 19 April 2022 doi:10.20944/preprints202204.0175.v1

frontal/prefrontal/anterior cingulate cortex error processing mechanisms may be important in motor skill learning since their activity is known to scale with motor error (Seidler et al., 2013). It has been proposed that an error related negativity signal with a prominent fronto-central radial voltage distribution (Wessel, 2012) is generated due to the negative reinforcement signal to the anterior cingulate cortex via the mesencephalic dopamine system (Holroyd and Coles, 2002). Then, the anterior cingulate cortex uses this negative reinforcement signal for corrective action (Holroyd and Coles, 2002), where subjective error awareness or perception may be critical (Wessel, 2012), i.e., in the absence of error perception, the corrective action will be missing. Then, the corrective action will activate the premotor areas for post-error adjustments (Perri et al., 2016). This error perception-action coupling is postulated for appropriate contextual switching of brain states that may be captured by the EEG microstates (Michel and Koenig, 2018).

Automatic corrective action will require learning the action semantics accompanied by implicit activation of motor representations (van Elk et al., 2009). The learned integration of the motor primitives can produce an appropriate effector's trajectory to reach the goal with high accuracy and precision. While there can be more than one trajectory of the body movement to perform a task (Vetter et al., 2002), there are only a few "efficient" trajectories. The efficient trajectory is learned while minimizing the task error over multiple trials of which only the experts have the 'executive memory.' Then, even with action semantic knowledge, lack of error perception, e.g., lack of medial frontal cortex activation on minor errors (Gehring and Fencsik, 2001), can disrupt skill learning. Therefore, this study aimed to evaluate a portable brain-behavior approach to capture the error-related scalp topographies or brain state changes subserving error processing and post-error adjustments during the FLS "suturing and intracorporeal knot-tying" task. Here, the change in the scalp topography during error processing and post-error adjustments immediately after the error even was analyzed as a “microstate” in the brain – defined as a short quasi-stable (60–120 ms) state – during which the scalp potential field from electroencephalogram (EEG) remains semi-stable (Michel and Koenig, 2018). Microstate analysis leverages the excellent temporal resolution of EEG (Michel and Koenig, 2018) and a meta-criterion on global field power (Skrandies, 1990), favoring the highest signal-to-noise ratio (Custo et al., 2017). Here, the proposed computational circuit mechanisms (Gu et al., 2021) have presented selective attention (Crick, 1984) or excitability alterations by the thalamus (Hughes et al., 2004) acting as a “spotlight” that can be postulated for error-related cognitive control (Ide and Li, 2011). The microstate approach for a correlate of motor control (Pirondini et al., 2017) has a crucial *a priori* assumption that only one spatial map entirely defines the relevant global state of the brain at each moment in time, and the residuals are considered noise.

Microstate analysis has been validated based on resting-state functional magnetic resonance imaging (fMRI), which has shown a close relationship in resting-state brain networks (Michel and Koenig, 2018) when combined with EEG source imaging. Since fMRI is challenging (Wanzel et al., 2007),(Leff et al., 2008a), during the FLS "suturing and intracorporeal knot-tying" task (henceforth, FLS complex task) so we combined EEG with functional near-infrared spectroscopy (fNIRS), which is a non-invasive optical imaging technique (Villringer et al., 1993) that exploits neurovascular coupling (like fMRI) to measure cortical activity. Combining fNIRS with EEG is beneficial since EEG can provide neural correlates of non-cortical brain regions at a high temporal resolution for microstate analysis, while fNIRS is limited to the cortical areas – a necessity to uncover cortical correlates of microstates to identify surgical expertise (Hannah et al., 2022). Here, EEG and fNIRS extract different physiological information about the brain activation – EEG measures the electromagnetic field generated by firing neurons while fNIRS measures the slower hemodynamic response. Therefore, microstate prototypes were selected from the excellent temporal resolution of EEG (Michel and Koenig, 2018) and the meta-criterion for global field power (GFP), favoring the highest signal-to-noise ratio (Custo et al., 2017). Then, the EEG band power changes corresponding to the oxyhemoglobin (HbO)

Preprints (www.preprints.org) | NOT PEER-REVIEWED | Posted: 19 April 2022 doi:10.20944/preprints202204.0175.v1

concentration changes from fNIRS data were found using regularized temporally embedded Canonical Correlation Analysis (tCCA) under the neurovascular coupling phenomenon (Sood et al., 2016),(Sirpal et al., 2021). This allowed analysis of the cortical activation based on HbO changes corresponding to the scalp topography of the EEG microstates following error events during the performance of the FLS complex task by experts and novices. While EEG detected fast changes under the limitations of volume conduction, fNIRS provided corresponding hemodynamic information over a longer timeframe with better localization of the cortical activity due to its limited spatial sensitivity. Given each modality's different characteristics and physiological information, the fusion of simultaneously acquired EEG and fNIRS signals is postulated to provide better mechanistic insights into the brain state changes during error perception and error correction. Moreover, human error processing (Holroyd and Coles, 2002) is postulated to differentiate experts from novices based on the differences in the error-related chain of mental processes captured with simultaneously acquired EEG-fNIRS based brain state analysis.

2. Materials and Methods

2.1. Subjects and task

After written consent, right-handed thirteen healthy novice medical students and nine expert surgeons were recruited for the study. The study was approved by the Institutional Review Board of the University at Buffalo, NY. All study procedures were performed according to local human subjects' research regulations. The experts (attending surgeons and residents) had greater than 1-year experience with laparoscopic tasks, whereas the novices (medical students) had never experienced the laparoscopic task. All the subjects were instructed verbally with a standard set of instructions on how to complete the FLS "suturing and intracorporeal knot-tying" task to the best of their capacity. Participants were provided with two laparoscopic needle drivers, one suturing scissors, and a needle with a suture of 15 cm in length. In this task, a Penrose drain with marked targets is placed on the Velcro strip inside the FLS box trainer. The subject has to tie three throws of a knot intracorporeally using two needle drivers, where the last two knots are single throws followed by a double throw, which closes the slit in the Penrose drain (Ritter and Scott, 2007). The task involves inserting the suture through two marks in a Penrose drain and then tying a double-throw knot followed by two single-throw knots using two needle graspers operated by both hands. The FLS task starts when the subject picks up the suture and needle driver on the ‘start’ command and ends when the subject cuts both ends of the suture, where the task completion is limited to 10 min (600 sec). The task was repeated three times along with 2 min of the rest period, and the ‘start’ and ‘stop’ triggers for the FLS task were manually registered with the data acquisition software. The experimenter labeled using the FLS box camera view of the error events at the “needle drop” and “incorrect needle insertion,” as shown in Figures 1 and 2, respectively. The multimodal imaging system using simultaneously acquired EEG and fNIRS signals recorded concurrent electrophysiological and hemodynamic responses of the brain while the subject performed the FLS complex task.

Preprints (www.preprints.org) | NOT PEER-REVIEWED | Posted: 19 April 2022 doi:10.20944/preprints202204.0175.v1

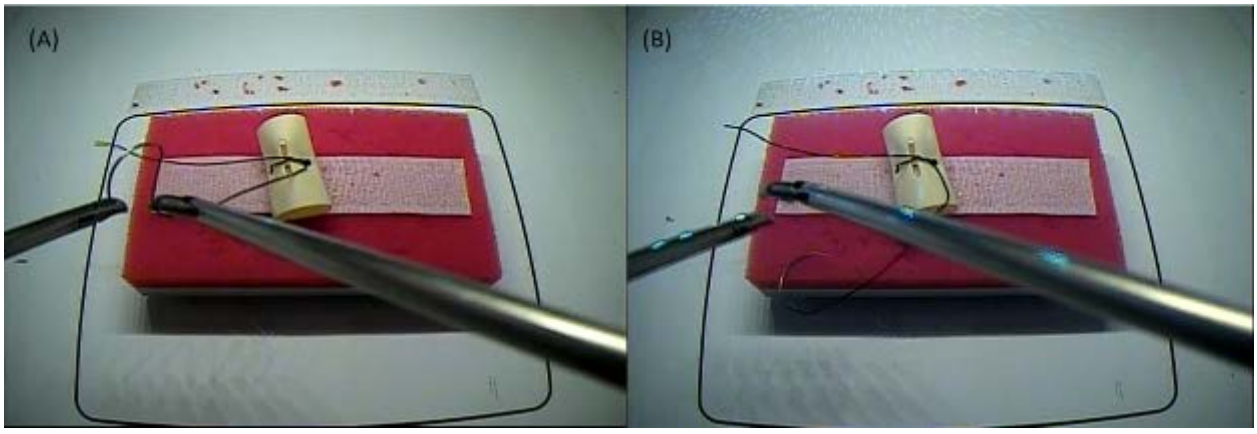

Figure 1. Image sequence showing "needle drop" error event during task performance.

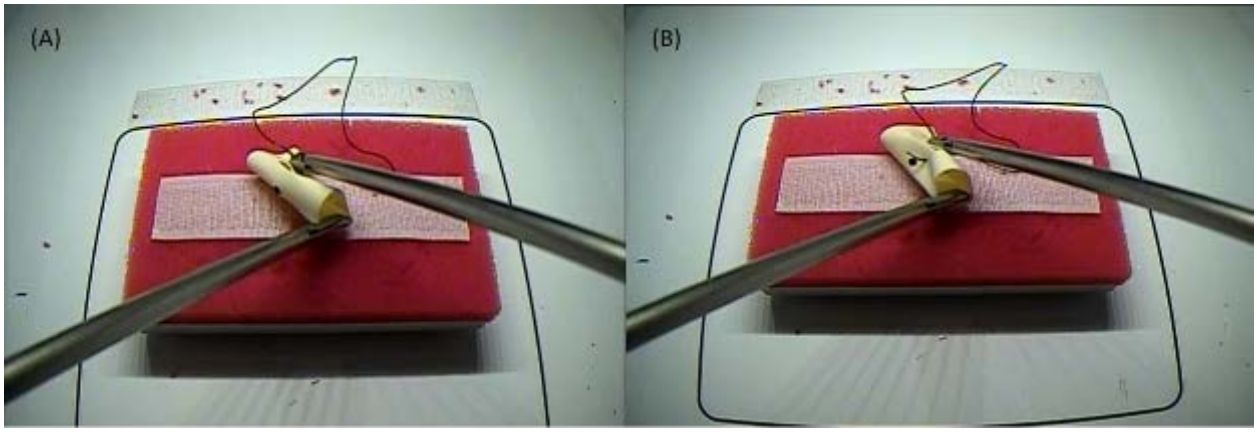

Figure 2. Image sequence showing "incorrect needle insertion" error event during task performance.

2.2. Synchronized multimodal portable brain imaging

A customized montage consisting of EEG electrodes and fNIRS optodes was used to record synchronized multimodal brain activation signals. 32-channel EEG signals were recorded using a wireless LiveAmp system (Brain Vision, USA). EEG recordings were obtained at 500 Hz using active gel-electrodes. 32-channel fNIRS signals along with 8-channel short-separation channels were recorded at a 5Hz sampling rate with NIRSPORT2 (NIRx, USA). A 1Hz hardware trigger signal implemented the fNIRS-EEG synchronization, and the multimodal data were aligned and epoched in 1-sec time windows. The optical probes and electrodes were located following standard 10-5 montage (see Figure 3A), with fNIRS probe sensitivity (Aasted et al., 2015) shown in Figure 3B. The probes were carefully placed on the subject's head to avoid hair interference and to not hinder the subject's mobility during the mobile brain-behavior study (see Figure 3C). Table 1 (from AtlasViewer software using its default head model) lists the labels of the fNIRS cortical region of interest (ROIs) that are based on the Automated Anatomical Labelling (AAL) atlas (Rolls et al., 2020, 3) and Montreal Neurological Institute (MNI) coordinate space (Aasted et al., 2015).

Preprints (www.preprints.org) | NOT PEER-REVIEWED | Posted: 19 April 2022 doi:10.20944/preprints202204.0175.v1

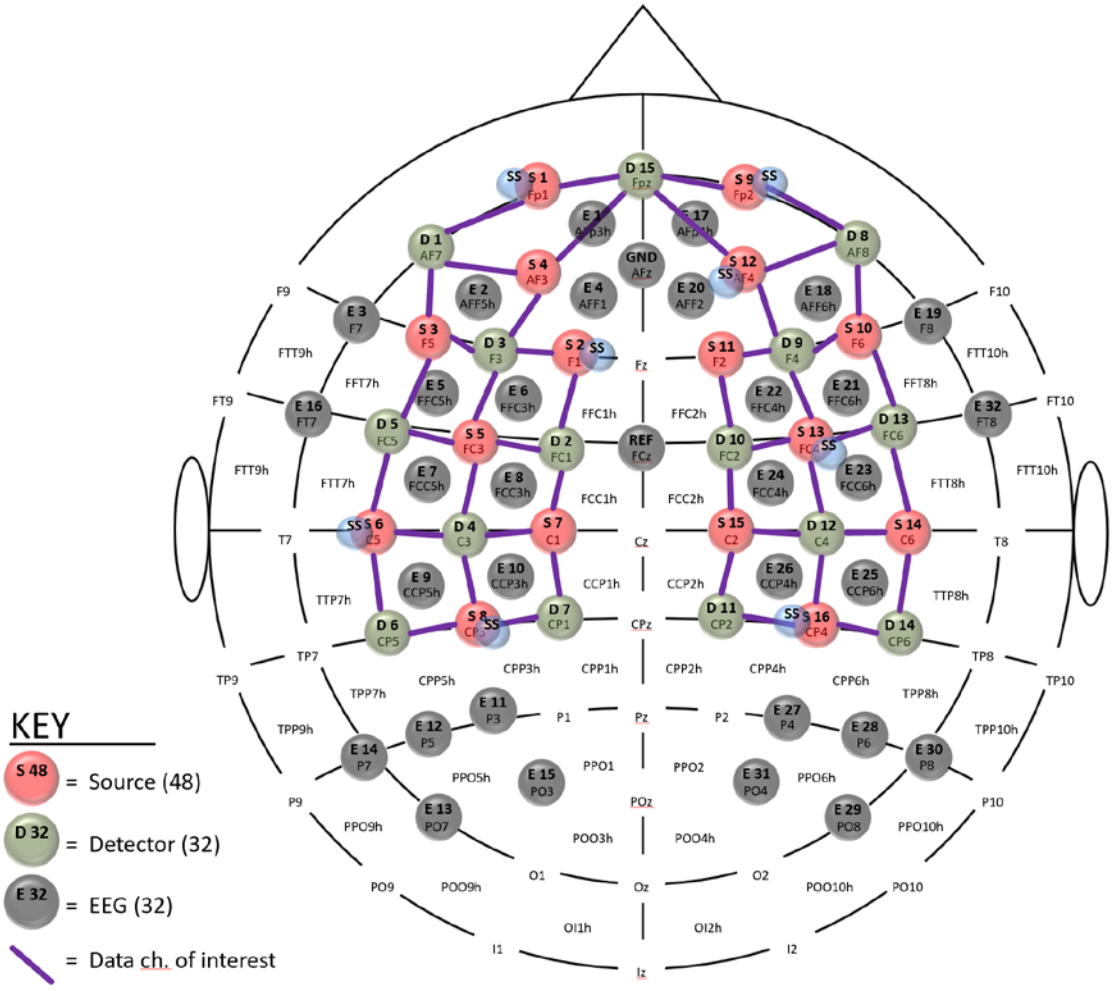

(A)

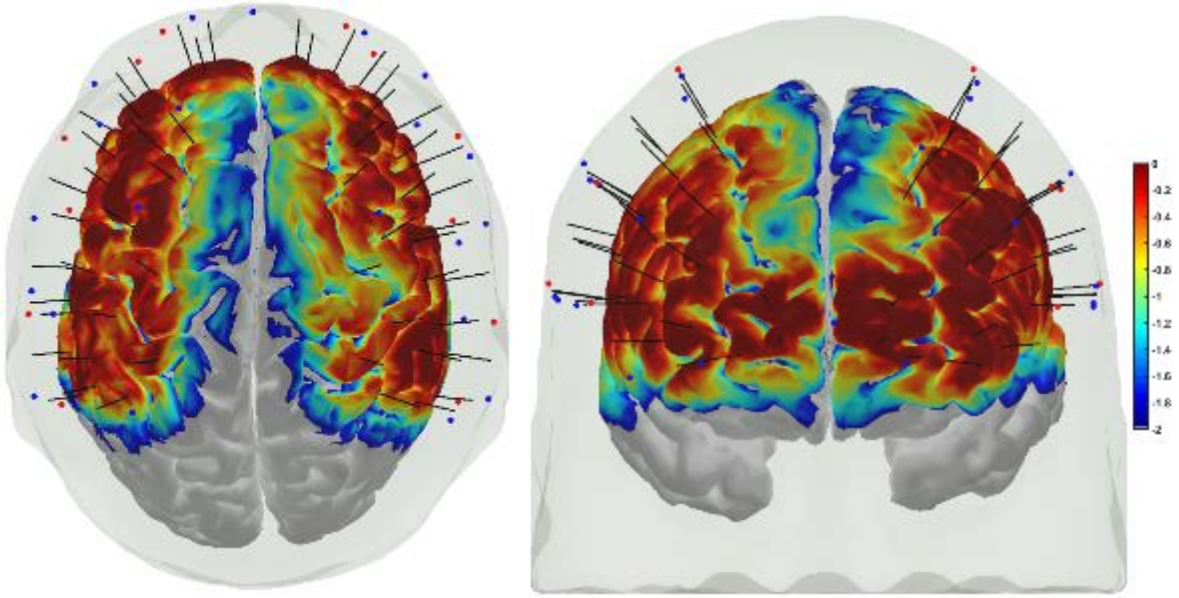

Preprints (www.preprints.org) | NOT PEER-REVIEWED | Posted: 19 April 2022 doi:10.20944/preprints202204.0175.v1

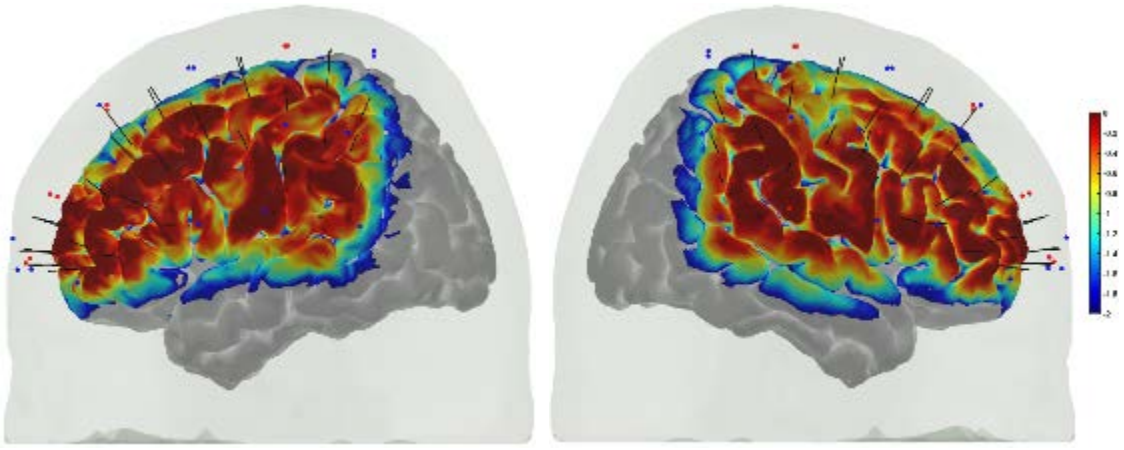

(B)

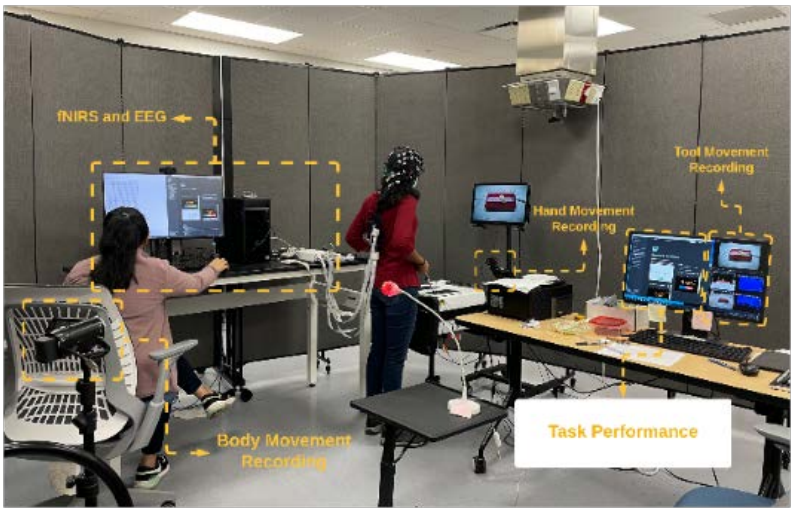

(C)

Figure 3. (A) Multi-modal (fNIRS-EEG) sensor montage including short-separation (labelled SS in light blue ellipeses) channels. The red filled circles are the fNIRS sources, the green filled circles are the fNIRS detectors, the grey filled circles are the EEG electrodes, the violet lines are the optode pairs for the fNIRS channels. (B) The probe sensitivity values in the 0.01 to 1 range are displayed logarithmically as −2 to 0 in log10 units in the color bar. The projection of the fNIRS channels on the cortex are shown with black arrows. (C) Experimental setup in the laboratory with the subject performing the FLS complex task.

Table 1. Automated anatomical labeling (AAL) and Montreal Neurological Institute (MNI) coordinates of the cortical areas underlying fNIRS channels (source # – detector # pair) when projected on the cortex in AtlasViewer using its default head model (Aasted et al., 2015).

Source #	Detector #	Channel Coordinates (MNI)	AAL label names
1	1	-30 56 -7	Frontal_Inf_Orb_L
1	15	-9 64 -8	Frontal_Sup_Orb_L
1	16	-11 57 -5	Frontal_Sup_Orb_L
2	2	-17 26 48	Frontal_Sup_L
2	3	-21 34 28	Frontal_Mid_L
2	17	-13 45 38	Frontal_Sup_L
3	1	-35 45 -2	Frontal_Inf_Orb_L
3	3	-30 33 20	Frontal_Mid_L

Preprints (www.preprints.org) | NOT PEER-REVIEWED | Posted: 19 April 2022 doi:10.20944/preprints202204.0175.v1

3	5	-36 8 13	Frontal_Inf_Oper_L
4	1	-38 55 -2	Frontal_Mid_Orb_L
4	3	-37 48 14	Frontal_Inf_Tri_L
4	15	-16 61 0	Frontal_Sup_Orb_L
5	2	-47 12 53	Frontal_Mid_L
5	3	-47 24 31	Frontal_Mid_L
5	4	-47 -9 41	Postcentral_L
5	5	-58 11 28	Precentral_L
6	4	-46 -23 34	Postcentral_L
6	5	-57 -11 15	Temporal_Sup_L
6	6	-37 -34 16	Rolandic_Oper_L
6	18	-63 -19 18	SupraMarginal_L
7	2	-27 -4 63	Frontal_Sup_L
7	4	-50 -22 63	Postcentral_L
7	7	-18 -34 57	Postcentral_L
8	4	-46 -30 47	Postcentral_L
8	6	-52 -49 34	SupraMarginal_L
8	7	-32 -47 54	Parietal_Inf_L
8	19	-29 -43 40	Parietal_Inf_L
9	8	41 57 -8	Frontal_Mid_Orb_R
9	15	15 67 -11	Frontal_Sup_Orb_R
9	20	21 54 -1	Frontal_Sup_R
10	8	47 47 -2	Frontal_Inf_Orb_R
10	9	51 37 18	Frontal_Inf_Tri_R
10	13	55 14 10	Frontal_Inf_Oper_R
10	21	44 19 8	Frontal_Inf_Tri_R
11	9	23 36 32	Frontal_Sup_R
11	10	33 34 56	Frontal_Sup_R
12	8	42 53 -1	Frontal_Mid_Orb_R
12	9	49 56 16	Frontal_Mid_R
12	15	18 62 -1	Frontal_Sup_Orb_R
13	9	53 24 32	Frontal_Inf_Tri_R
13	10	45 9 47	Precentral_R
13	12	57 -7 46	Precentral_R
13	13	58 9 26	Precentral_R
13	22	48 6 38	Precentral_R
14	12	63 -20 36	SupraMarginal_R
14	13	43 -8 18	Insula_R
14	14	46 -35 18	Temporal_Sup_R
15	10	36 -7 64	Frontal_Sup_R
15	11	39 -38 76	Postcentral_R
15	12	41 -22 52	Precentral_R
16	11	42 -49 57	Parietal_Sup_R
16	12	51 -33 49	SupraMarginal_R
16	14	45 -46 34	Angular_R
16	23	35 -46 42	Angular_R

2.3. fNIRS-EEG data preprocessing

The simultaneously recorded EEG and fNIRS signals were preprocessed and analyzed offline. The EEG signals were preprocessed using the open-source EEGlab toolbox (https://sccn.ucsd.edu/eeglab/index.php) for the microstate analysis (Michel and Koenig, 2018). Specifically, the data were downsampled to 250Hz and high-pass filtered at 1Hz. Then, the line noise was removed using 'cleanline' function, followed by 'clean_rawdata' function to reject bad channels. The bad channels were interpolated using spherical splines (Perrin et al., 1989) in 'clean_rawdata' followed by re-referencing to the

Preprints (www.preprints.org) | NOT PEER-REVIEWED | Posted: 19 April 2022 doi:10.20944/preprints202204.0175.v1

global average. Artifact subspace reconstruction (ASR) was performed using the default settings in EEGlab, followed by re-referencing to the global average. ASR is an automated method based on a user-specified parameter that can effectively remove transient EEG artifacts (Chang et al., 2020). We used the default ASR parameter value of 20, and the optimal value is between 20 and 30 to balance between removing non-brain signals and retaining brain activities (Chang et al., 2020). In this study's preprocessed EEG data used (13 novices and 8 experts) for microstate analysis, the maximum number of bad channels for any subject was less than five, where we rejected one expert subject. Then, Laplacian spatial filter was applied to remove the volume conduction from subcortical sources and keep the cortical sources that corresponded with cortical hemodynamic response measured with the fNIRS. Preprocessing of the fNIRS data was performed using the standard open-source HOMER3 package (https://github.com/BUNPC/Homer3). The fNIRS preprocessing pipeline is the following: first intensity was converted to optical density and then motion artifacts were detected and filtered with the help of the Savitzky-Golay filtering method (Jahani et al., 2018) with default parameters in HOMER3. Then, the optical density was bandpass filtered in the neurovascular coupling band, 0.01-0.1Hz, and then converted to chromophore (HbO) concentration with unit partial pathlength factor.

2.4. Error-related fNIRS-EEG microstates analysis

Microstate analysis was performed using the EEGlab toolbox (Poulsen et al., 2018) after aggregating EEG data during the FLS complex task from all the experts and novices. First, we identified EEG microstate prototypes based on modified K-means clustering in the EEGlab. The modified K-means clustering was based on goodness of fit of the microstate segmentation determined from the global explained variance (GEV) and the cross-validation criterion (CV). Here, the GEV criterion should theoretically become monotonically larger with the increasing number of clusters (Poulsen et al., 2018). The modified K-means clustering in EEGlab finds topographical maps of polarity invariant microstate prototypes (Poulsen et al., 2018) from the spontaneous EEG data during the FLS complex task (and rest periods in between the trials) . Here, global field power (GFP) peaks are used to segment the spontaneous EEG. The minimum peak distance was set at 10ms (default) and 1000 randomly selected peaks (default) per subject were used for the segmentation. Then, we rejected the GFP peaks that exceeded one time the standard deviation of all the GFPs of all maps to segment the EEG data into a predefined number (2 to 8) of microstates. Here, the goal is to maximize the similarity between the EEG samples and the prototypes of the microstates they are assigned to using the modified K-means algorithm (Poulsen et al., 2018). The modified K-means algorithm also sorts the microstate prototypes in decreasing GEV. We had set 100 random number of initializations and 1000 maximum number of iterations for the modified K-means algorithm with the 1e-6 (default) as the relative threshold of convergence (Poulsen et al., 2018). These microstates provided the prototypes for the subsequent error-related microstate analysis. The error epochs were defined for the 10sec following the error event at needle drop or incorrect needle insertion. Here, a 10-sec epoch was chosen for the error evoked fNIRS-EEG data to capture the EEG band power (1-40Hz) changes corresponding to hemodynamic response function since the maximum fNIRS frequency is 0.1 Hz in the neurovascular coupling band (i.e., a time period of 10 sec). Also, prior work (Li et al., 2020) showed that the HbO concentration peaked in the time range of 3-9 seconds for complex motor action, so 10-sec duration was considered adequate.

Microstate labels were applied to the EEG samples from the error epochs based on topographical similarity (called backfitting) using the EEGlab toolbox (Poulsen et al., 2018). Since short periods of unstable EEG topographies can occur so, we applied temporal smoothing. Then, the statistical properties of the EEG microstates were computed and used to compare error-related cortical activation between the experts and the novices. To find the corresponding hemodynamic response under neurovascular

Preprints (www.preprints.org) | NOT PEER-REVIEWED | Posted: 19 April 2022 doi:10.20944/preprints202204.0175.v1

coupling, the correspondence between the fNIRS HbO changes and the EEG band power (1-40Hz) changes were found based on the General Linear Model (GLM) and regularized Canonical Correlation Analysis with temporal embedding in HOMER3 (von Lühmann et al., 2020). The evoked hemodynamic signal is typically reconstructed with a weighted set of temporal basis functions in HOMER3 (von Lühmann et al., 2020); however, we reconstructed the HbO response from multi-channel EEG band power (1-40Hz) signals. Here, the design matrix consists of all the regressors for GLM that are solved with a least-squares approach for each regressor's contribution based on their coefficients (von Lühmann et al., 2020), so, the coefficients of the EEG band power (1-40Hz) regressors were used reconstruct the corresponding hemodynamic signal (HbO time series). The GLM approach also captures systemic artefacts with short-separation (SS) fNIRS channels as regressors and a 3rd order polynomials to model drift. So, the SS fNIRS channels served as the nuisance regressors for the systemic artefact in the design matrix (von Lühmann et al., 2020). However, identification of the EEG band power (1-40Hz) regressors from multi-channel EEG data is a challenge and we used 'hmrR_tCCA' function in HOMER3 to find the neurovascular coupling in the latent space (Rezaee et al., 2021) between the HbO time series at all the long-separation (LS) fNIRS channels and the simultaneously acquired EEG band power (1-40Hz) signals from all the EEG electrodes. Here, we selected 15 regressors from simultaneously acquired EEG band power (1-40Hz) signals that have a canonical correlation greater than the threshold, 0.99 (=param.ct in the function, 'rtcca'). Therefore, regularized Canonical Correlation Analysis with temporal embedding (tCCA) found fifteen regressors (shown in Supplementary Materials) from EEG band power (1-40Hz) signals to reconstruct the corresponding fNIRS signal from the LS channels while regressing out the SS fNIRS signal representing systemic artefacts using the GLM approach. The flowchart of the processing pipeline is shown in Figure 4.

The hemodynamic (HbO) response (10sec) during the FLS complex task and the error epoch was subjected to t-tests to detect significant ($p<0.05$) differences between experts and novices (i.e., skill level) for each fNIRS channel after controlling for the false discovery rate (FDR). The Matlab function 'hmrG_t_HRF_contrast2' and 'fdr_bh' for t-test and FDR are presented in the Supplementary Materials. Then, the visualization of the hemodynamic (HbO) response was performed using the AtlasViewer (Aasted et al., 2015). Also, the temporal property of the backfitted microstates of each subject, i.e., the proportion of the total time spent in six microstates (Poulsen et al., 2018), was extracted during the FLS complex task and the error epoch for the two-way analysis of variance (ANOVA) with factors, skill level (expert, novice) and microstate types, after testing for normality with Shapiro Wilks Test. The significance level was set at $\alpha=0.05$.

3. Results

We selected six EEG microstate prototypes based on the GEV and the CV criterion, as shown in Figure 5A. Here, the CV criterion, pointing to the best clustering solution at its smallest value, reached the minimum value for six microstates that are shown in Figure 5B, sorted in decreasing GEV. As expected for a visuomotor task, the highest GEV is for the microstate 1, corresponding to the activation of the visual cortex (and visual imagery (Britz et al., 2010)). The six microstate prototypes were backfitted to the EEG for 10 sec at the start of the FLS complex task and during the error epoch shown in Figure 6 for an expert and a novice. There were five error epochs in the expert group (N=8), whereas there were ten error epochs in the novice group (N=13).

Figure 6A and 6B show the GFP of the active states from 0 to 10000 ms at the start of the FLS complex task for a novice and expert, respectively, while Figure 6C and 6D show the GFP of the active states from 0 to 10000 ms during the error epoch of a novice and an expert respectively. In the illustrative examples shown in the Figure 6, the first 10 sec of error processing related brain states were captured in the expert (Figure 6D) by the microstate 1 (corresponding to the activation of the visual cortex (Britz et al., 2010)), microstate 3 (corresponding to the attention reorientation (Britz et al., 2010) and medial

Preprints (www.preprints.org) | NOT PEER-REVIEWED | Posted: 19 April 2022 doi:10.20944/preprints202204.0175.v1

frontal cortex activation related to error (Gehring and Fencsik, 2001)), the microstates 4 and 5, while the novice had the activation of microstates 1, 2, 3, and 5 (Figure 6C) during 10 sec of error processing.

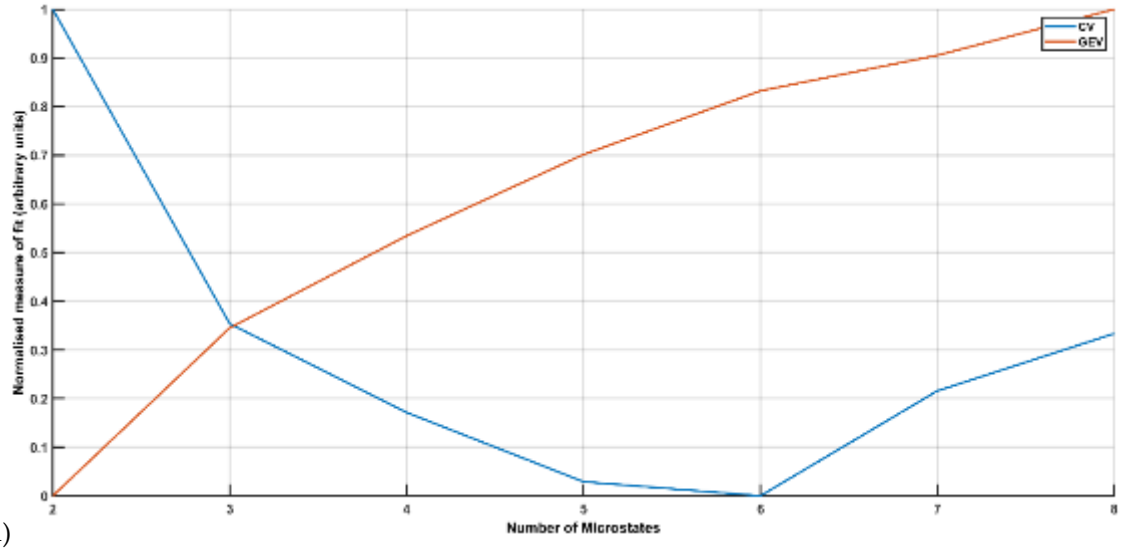

(A)

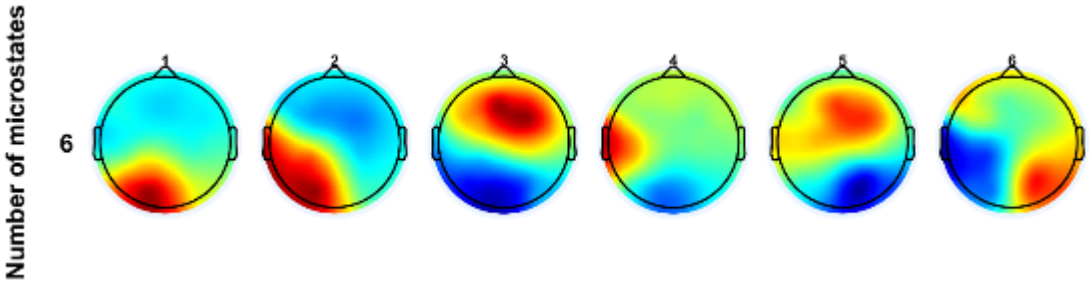

(B)

Figure 5. (A) Measures of fit plotted for the different microstate segmentations based on the global explained variance (GEV) and the cross-validation criterion (CV). (B) The selected six microstate prototypes based on the GEV and the CV criterion that are sorted in decreasing GEV.

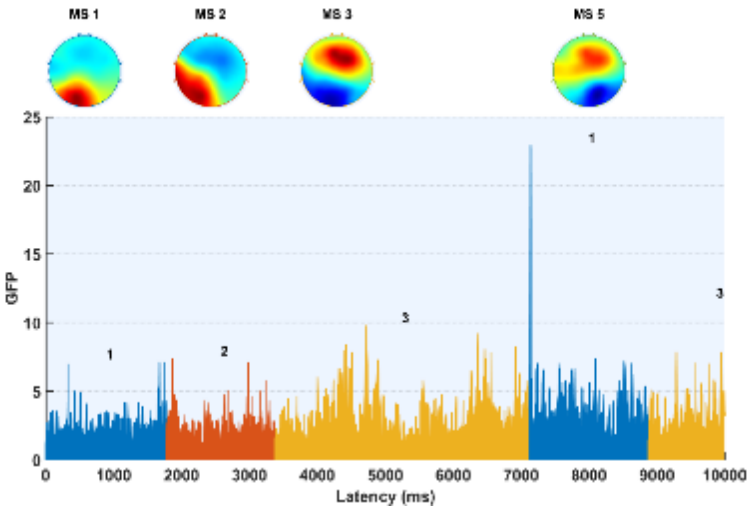

(A)

Preprints (www.preprints.org) | NOT PEER-REVIEWED | Posted: 19 April 2022 doi:10.20944/preprints202204.0175.v1

(B)

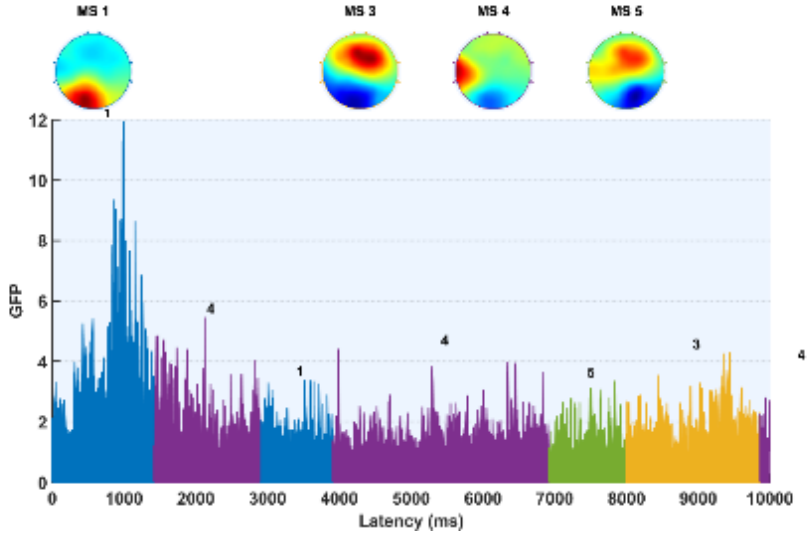

(C)

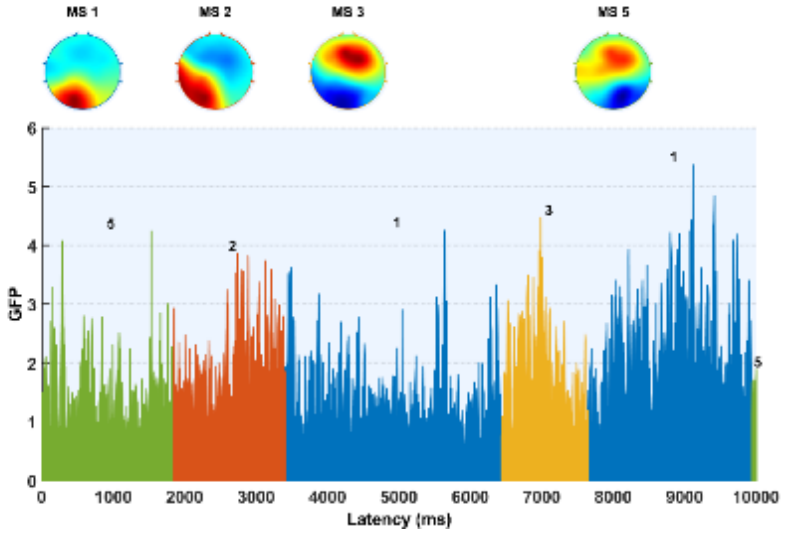

(D)

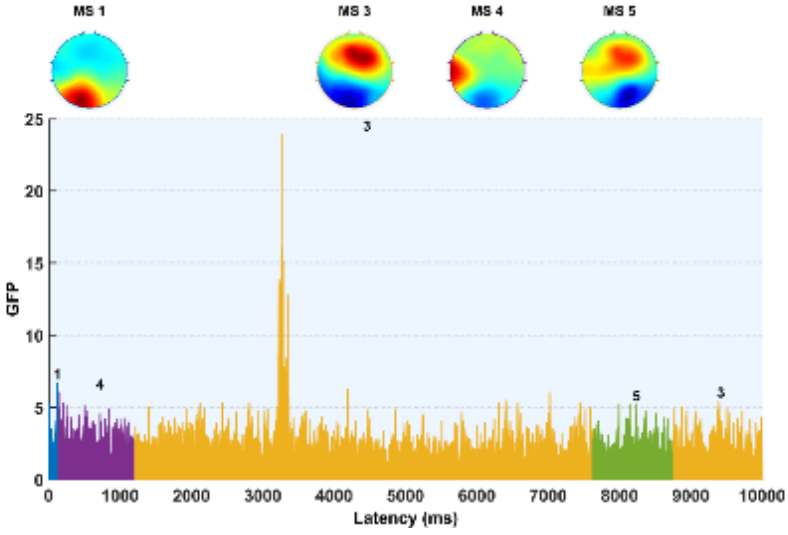

Figure 6. Illustrative figure of the GFP of active microstates, (A) during 0 to 10000 ms at the start of the FLS complex task of the EEG of a novice, (B) during 0 to 10000 ms at the start of the FLS complex task of the EEG of an expert, (C) during 0 to 10000 ms during the error epoch of the EEG of a novice, (D) during 0 to 10000 ms during the error epoch of the EEG of an expert.

Preprints (www.preprints.org) | NOT PEER-REVIEWED | Posted: 19 April 2022 doi:10.20944/preprints202204.0175.v1

Overall, novices had a more widespread cortical activation during the error epoch compared to the experts, which is evident from the image of the corresponding changes in the HbO absorption coefficient in the cortex (Aasted et al., 2015). Here, we computed the EEG band power (1-40Hz) related changes in the HbO signals using GLM and regularized temporally embedded Canonical Correlation Analysis (von Lühmann et al., 2020) in HOMER3. Then, the image of the changes in the HbO absorption coefficient in the cortex (Aasted et al., 2015) of the experts and novices during the 10 sec at the start of the FLS complex task and during the error epoch are shown in Figure 7.

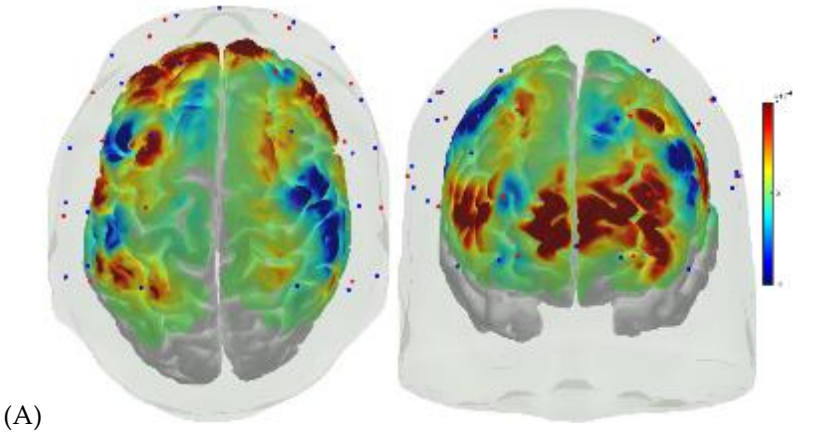

(A)

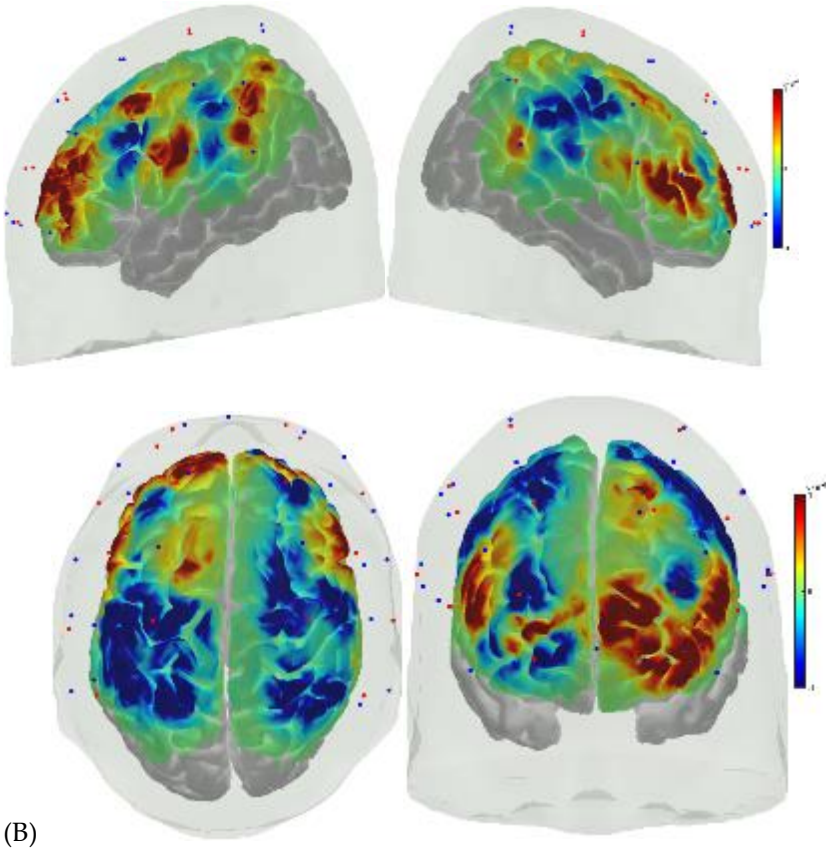

(B)

Preprints (www.preprints.org) | NOT PEER-REVIEWED | Posted: 19 April 2022 doi:10.20944/preprints202204.0175.v1

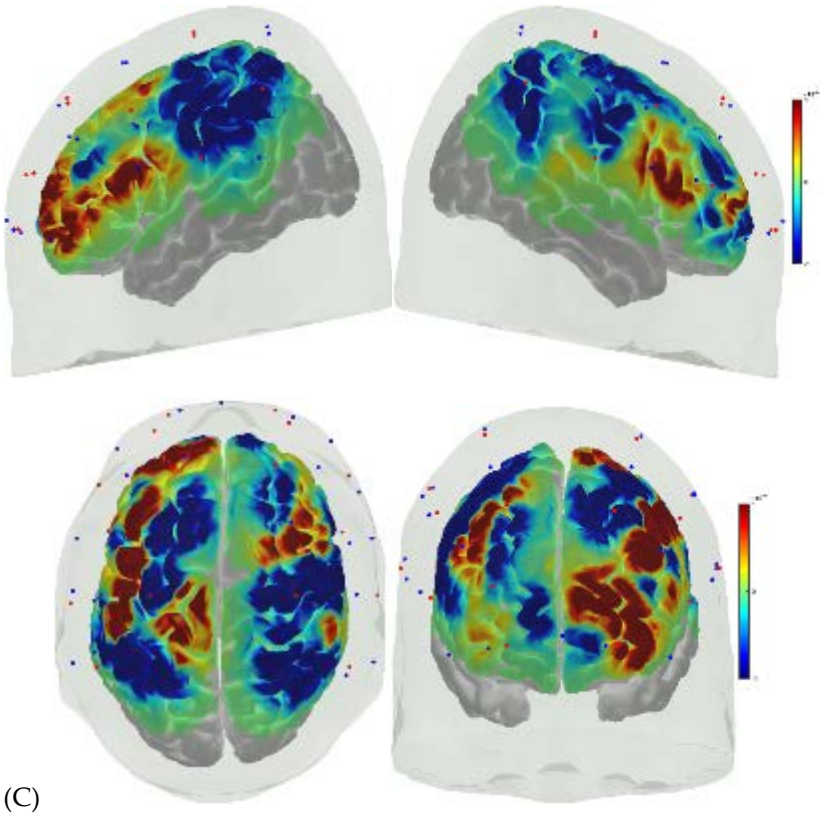

(C)

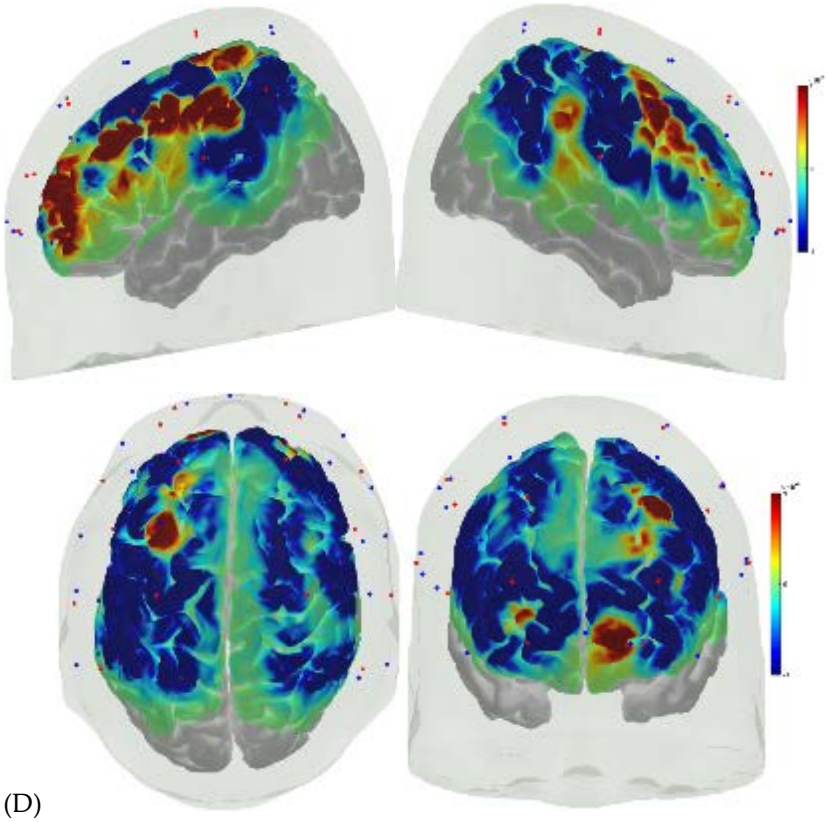

(D)

Preprints (www.preprints.org) | NOT PEER-REVIEWED | Posted: 19 April 2022 doi:10.20944/preprints202204.0175.v1

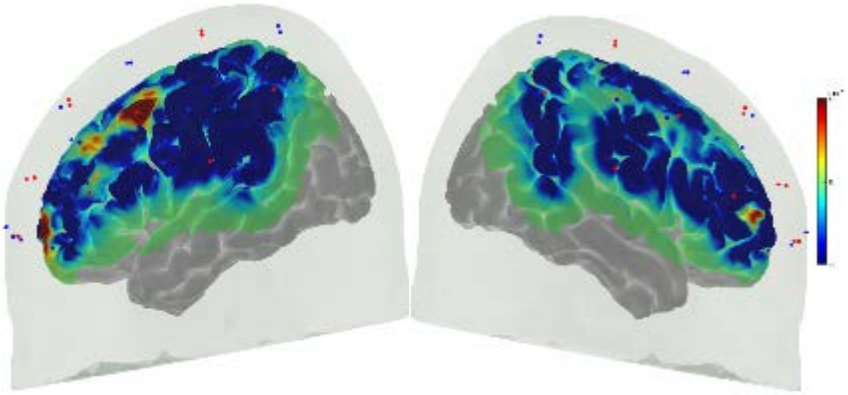

Figure 7. Image of the changes in HbO absorption coefficient in the cortex, (A) during 0 to 10 sec at the start of the FLS complex task of the novices, (B) during 0 to 10 sec at the start of the FLS complex task of the experts, (C) during 0 to 10 sec during the error epoch of the novices, (D) during 0 to 10 sec during the error epoch of the experts.

Table 2. Difference (p-value) in the hemodynamic (HbO) response across all fNIRS channels between the novices and the experts during 0 to 10 sec at the start of the FLS complex task and in the error epoch. Automated anatomical labelling (AAL) of the cortical areas underlying fNIRS channels (source # – detector # pair) are also listed based on AtlasViewer's default head model (Aasted et al., 2015).

Source #	Detector #	AAL label names	FLS complex task – p value	Error epoch – p value
1	1	Frontal_Inf_Orb_L	0.78	0.35
1	15	Frontal_Sup_Orb_L	0.95	0.69
1	16	Frontal_Sup_Orb_L	0.64	0.79
2	2	Frontal_Sup_L	0.35	0.77
2	3	Frontal_Mid_L	0.59	0.78
2	17	Frontal_Sup_L	0.45	0.17
3	1	Frontal_Inf_Orb_L	0.45	0.27
3	3	Frontal_Mid_L	0.17	0.67
3	5	Frontal_Inf_Oper_L	0.14	0.03*
4	1	Frontal_Mid_Orb_L	0.84	0.04*
4	3	Frontal_Inf_Tri_L	0.19	0.56
4	15	Frontal_Sup_Orb_L	0.71	0.29
5	2	Frontal_Mid_L	0.59	0.54
5	3	Frontal_Mid_L	0.80	0.08
5	4	Postcentral_L	0.11	0.11
5	5	Precentral_L	0.41	0.23
6	4	Postcentral_L	0.04*	0.04*
6	5	Temporal_Sup_L	0.37	0.01*
6	6	Rolandic_Oper_L	0.77	0.44
6	18	SupraMarginal_L	0.46	0.34
7	2	Frontal_Sup_L	0.74	0.89
7	4	Postcentral_L	0.04*	0.48
7	7	Postcentral_L	0.18	0.42
8	4	Postcentral_L	0.16	0.23
8	6	SupraMarginal_L	0.23	0.73
8	7	Parietal_Inf_L	0.14	0.44
8	19	Parietal_Inf_L	0.59	0.51
9	8	Frontal_Mid_Orb_R	0.33	0.04*
9	15	Frontal_Sup_Orb_R	0.04*	0.44
9	20	Frontal_Sup_R	0.88	0.23
10	8	Frontal_Inf_Orb_R	0.34	0.11
10	9	Frontal_Inf_Tri_R	0.23	0.14
10	13	Frontal_Inf_Oper_R	0.80	0.09
10	21	Frontal_Inf_Tri_R	0.79	0.78

Preprints (www.preprints.org) | NOT PEER-REVIEWED | Posted: 19 April 2022 doi:10.20944/preprints202204.0175.v1

11	9	Frontal_Sup_R	0.44	0.97
11	10	Frontal_Sup_R	0.05	0.80
12	8	Frontal_Mid_Orb_R	0.64	0.19
12	9	Frontal_Mid_R	0.32	0.15
12	15	Frontal_Sup_Orb_R	0.47	0.32
13	9	Frontal_Inf_Tri_R	0.78	0.45
13	10	Precentral_R	0.34	0.72
13	12	Precentral_R	0.57	0.35
13	13	Precentral_R	0.47	0.62
13	22	Precentral_R	0.71	0.89
14	12	SupraMarginal_R	0.34	0.59
14	13	Insula_R	0.81	0.71
14	14	Temporal_Sup_R	0.40	0.77
15	10	Frontal_Sup_R	0.17	0.45
15	11	Postcentral_R	0.05	0.54
15	12	Precentral_R	0.85	0.14
16	11	Parietal_Sup_R	0.18	0.69
16	12	SupraMarginal_R	0.83	0.86
16	14	Angular_R	0.59	0.82
16	23	Angular_R	0.57	0.23

The backfitting of the microstate prototypes (shown in Figure 5B) to all the data points during 10 sec at the start of the FLS complex task explained 64.29% GEV in novices and 73.64% GEV in the experts, while backfitting of the microstate prototypes to all the data points during 10 sec in the error epoch explained 58.98% GEV in novices and 65.96% GEV in the experts. Figure 8A shows the ANOVA table where the proportion of the total time spent in microstates during the 10 sec at the start of the FLS complex task was significantly affected by the skill level (experts, novices) and the interaction between the skill level and the microstate (MS1-MS6) at α=0.05. Then, Figure 8B shows the ANOVA table where the proportion of the total time spent in microstates during the 10-sec error epoch was significantly affected by the skill level ($p<0.01$), microstates ($p<0.01$), and the interaction between the skill level and the microstate ($p<0.01$).

(A)

Analysis of Variance

Source	Sum Sq.	d.f.	Mean Sq.	F	Prob>F
skill level	0.05061	1	0.05061	7.58	0.0068
microstate	0.04827	5	0.00965	1.45	0.2127
skill level*microstate	0.08372	5	0.01674	2.51	0.0338
Error	0.80113	120	0.00668		
Total	0.99137	131			

(B)

Analysis of Variance

Source	Sum Sq.	d.f.	Mean Sq.	F	Prob>F
skill level	0.02834	1	0.02834	22.29	6.41568e-06
microstate	0.11654	5	0.02331	18.33	1.73555e-13
skill level*microstate	0.19494	5	0.03899	30.66	5.4958e-20
Error	0.15258	120	0.00127		
Total	0.52815	131			

Figure 8. (A) The proportion of the total time spent in microstates (MS) during 10 sec at the start of the FLS complex task was significantly affected by the skill level (experts, novices) and the interaction between the skill level and the microstate (MS1-MS6) at α=0.05. (B) The proportion of the total time spent in microstates during the 10-sec error epoch was

Preprints (www.preprints.org) | NOT PEER-REVIEWED | Posted: 19 April 2022 doi:10.20944/preprints202204.0175.v1

significantly affected by the skill level (experts, novices), microstates (MS1-MS6), and the interaction between the skill level and the microstates at α=0.05.

While microstate prototypes were computed from EEG data with a high temporal resolution, the corresponding fNIRS (HbO) activity is a low-pass filtered version (under neurovascular coupling) shown as changes in the HbO absorption coefficient in the cortex in Figure 7. Here, a significant difference ($p<0.05$) in the hemodynamic (HbO) response between the novices and the experts across fNIRS channels (listed in Table 1) during 0 to 10 sec at the start of the FLS complex task and in error epoch is shown with '*' in Table 2. During the FLS complex task, HbO signal from the fNIRS channel overlying 'Postcentral_L' and 'Frontal_Sup_Orb_R' cortical areas from Automated anatomical labelling (AAL) showed a significant ($p<0.05$) difference whereas HbO signal from fNIRS channel overlying 'Frontal_Inf_Oper_L', 'Frontal_Mid_Orb_L', 'Postcentral_L', 'Temporal_Sup_L', 'Frontal_Mid_Orb_R' cortical areas from AAL showed significant ($p<0.05$) difference in the error epoch.

4. Discussion

In this study, we aimed to show the fusion of simultaneously acquired EEG and fNIRS signals to provide better mechanistic insights into the changes in the brain state during error perception and correction. Indeed, EEG based microstate analysis provided insights based on the scalp topography of the microstates, as shown by illustrative examples of the GFP of the active microstates in Figure 6, where microstate 2 was only present in the novice while the microstate 4 was present in the expert during the first 10 sec of the FLS complex task and the error epoch. Here, the scalp topography showed left lateralization in the right-handed subjects. Then, the corresponding HbO response and the image of the changes in HbO absorption coefficient in the cortex are shown in Figure 7. Here, we postulated that the simultaneously acquired EEG-fNIRS-based brain state analysis would be able to differentiate experts from novices. Indeed, statistical testing of the HbO hemodynamic response at the fNIRS channels identified underlying 'Postcentral_L' and 'Frontal_Sup_Orb_R' AAL cortical areas as significantly different between the experts and novices during 10 sec at the start of the FLS complex task while HbO hemodynamic response at the underlying 'Frontal_Inf_Oper_L', 'Frontal_Mid_Orb_L', 'Postcentral_L', 'Temporal_Sup_L', 'Frontal_Mid_Orb_R' AAL cortical areas were significantly different between experts and novices during the error epoch. Here, we postulate that the frontal/prefrontal cortical areas are related to the perception, and the primary somatosensory cortex at the postcentral cortical area is related to the action towards perception-action coupling model at the start of the FLS complex task as well as in the error epoch.

Numerous functional magnetic resonance imaging (fMRI) and fNIRS studies have been published on skill learning (Roberts et al., 2006)·(Ohuchida et al., 2009)·(Leff et al., 2008c)·(Wanzel et al., 2007)·(Leff et al., 2007)·(Gao et al., 2021a)·(Leff et al., 2008b)·(Khoe et al., 2020)·(Gao et al., 2021b). Although fMRI studies have shown that a large-scale brain network can encode the motor learning and transfer of learning from past experiences (Heitger et al., 2012)·(Gerraty et al., 2014); however, fMRI is not suitable for mobile brain-behavior studies. The prefrontal cortex (PFC) has been found to integrate the information necessary for action generation and action perception (Raos and Savaki, 2017). Future studies need to investigate error-related pupil dilation (Maier et al., 2019) in conjunction with EEG microstate, e.g., canonical subjective interoceptive-autonomic processing (Britz et al., 2010) may be a marker of error sensitivity. A future longitudinal study on FLS complex task learning can investigate the postulated error sensitivity to drive learning in novice – fast learners versus slow learners. Here, EEG microstate transitions can provide insights into the learning-related mental processes. In this study, the time spent in microstates during the 10 sec at the start of the FLS complex task was significantly affected by the skill level (experts, novices) and the interaction between the skill level and the

Preprints (www.preprints.org) | NOT PEER-REVIEWED | Posted: 19 April 2022 doi:10.20944/preprints202204.0175.v1

microstate types at α=0.05. Also, the proportion of the total time spent in microstates during the 10 sec error epoch was significantly affected by the skill level, microstates type, and the interaction between the skill level and the microstate type at α=0.01. Therefore, brain states underpinning human error processing (Holroyd and Coles, 2002) and the error-related chain of mental processes captured by the microstates could differentiate experts from novices better at α=0.01. We found microstates 3 and 5 to be present in both experts and novices that may be related to error evaluation mechanisms in the medial frontal cortex. Here, combining pupil dilation with EEG microstate analysis in the error epoch may elucidate the mechanisms underlying error-related pupil dilation during skill training – fast versus slow learners. This is important since FLS task performance is graded based on the speed and accuracy of psychomotor skills (Ritter and Scott, 2007); however, not everyone can achieve proficiency (Grantcharov and Funch-Jensen, 2009). Here, we postulate that successful skill acquisition leads to an internal forward model (Wolpert et al., 1998) that can simulate the perceptual consequences of the planned and executed motor commands. An intact action-perception coupling that is relevant for surgical skill acquisition has been shown to depend on the integrity of the cerebellum (Christensen et al., 2014) that underpins the internal model (Ebner, 2013). Then, the hierarchy of cognitive control during skill learning shows a rostrocaudal axis in the frontal lobe (Badre and D'Esposito, 2009a), where a shift from posterior to anterior is postulated to mediate progressively abstract, higher-order control expected in the experts. Here, the dorsolateral and ventrolateral PFC showed activation in Figure 7A,B during the FLS complex task that can be related to attention control, cognitive control, feature extraction, and formation of first-order relationships (Badre and D'Esposito, 2009b),(Badre, 2008),(Koechlin and Summerfield, 2007),(Christoff and Gabrieli, 2000). Specifically, the dorsolateral PFC of the dorsal stream is more involved in the visual guidance of action in novices (Figure 7A). In contrast, the ventrolateral PFC of the ventral stream is more involved in the recognition and conscious perception (Milner, 2017) in experts (Figure 7B). Then, the supplementary motor area (SMA) and the premotor cortex are crucial for the coordination of bimanual movement (Tanji et al., 1988), where SMA is crucial for complex spatiotemporal sequencing of movements (Debaere et al., 2004)·(Swinnen and Wenderoth, 2004) necessary in bimanual FLS complex task (Figure 7B). Also, the cingulate and pre-supplementary motor areas are the generator sites of error-related negativity. This event-related potential component is time-locked to an erroneous response (Seidler et al., 2013). Then, SMA is involved in planning complex motor finger tasks (PE et al., 1980), critical in error correction (Seidler et al., 2013).

Brain-behavior monitoring of the error-related cortical activation and corrective action can allow appropriate error feedback for operant conditioning in future work that has been shown feasible in our prior application for stroke rehabilitation (Kumar et al., 2019). For example, some novices' lack of error perception (i.e., lack of medial frontal cortex activation on minor errors (Gehring and Fencsik, 2001)) can disrupt their skill learning, which can be improved with its non-invasive brain stimulation in conjunction with explicit error feedback in the medical simulator. Here, microstate 3 can be related to the attention reorientation (Britz et al., 2010) and medial frontal cortex activation related to error (Gehring and Fencsik, 2001) in the novice, while the microstate 4 can be associated with the activation of the left inferior parietal lobe (Numssen et al., 2021) since experts have the action semantics knowledge (van Elk, 2014). Therefore, EEG topographies provide subject-specific correlates of motor control (Pirondini et al., 2017), and portable neuroimaging guided non-invasive brain stimulation may be feasible to facilitate skill training (Walia et al., 2021a). Here, perception and action together form a functional system that adapts novice behavior during motor learning. The two crucial attributes of the perception-action cycle are perceptual and executive memory (Fuster, 2004), where error sensitivity is postulated to depend on the memory of errors (the history of past consistent errors) (Albert et al., 2021) that drives skilled error correction (Seidler et al., 2013). For example, early efferent error prediction can lead to immediate adjustments in

Preprints (www.preprints.org) | NOT PEER-REVIEWED | Posted: 19 April 2022 doi:10.20944/preprints202204.0175.v1

experts, e.g., skilled typists execute errors with lighter keystrokes than novices. Published studies have shown that the pre-supplementary motor area (pre-SMA) and the inferior frontal gyrus are involved in stop-signal task performance (Seidler et al., 2013). Then, in our prior work (Walia et al., 2021a) on portable neuroimaging during the FLS complex task, we found that the average cortical activation was primarily at the left pars opercularis of the inferior frontal gyrus involved in cognitive control (Levy and Wagner, 2011). In contrast, the left frontopolar prefrontal area was more active in the experts (Figure 7B).

This study used portable brain imaging with fNIRS that have limited spatial and depth sensitivity (Strangman et al., 2013). Published fNIRS studies showed the involvement of the inferior parietal cortex, PFC, occipital cortex, and the sensorimotor areas, including the premotor and primary motor cortex. In contrast, the fMRI studies showed additional activation of deeper brain structures, including the basal ganglia and cerebellum (Roberts et al., 2006). The limitation of our study includes a low-density fNIRS and EEG sensor montage that limited the spatial resolution. It is known from skill learning studies that the hierarchy of cognitive control shows a rostrocaudal axis in the frontal lobe where a shift from posterior to anterior is postulated to mediate progressively abstract, higher-order control [30, p. 707], which requires a higher-density whole-head montage. Multimodal imaging limited the head cap space available for high-density portable imaging with our separate optodes and electrodes montage, where an integrated "co-located" optode+electrode (optrode) can be helpful (Keles et al., 2016) in future studies.

Author Contributions

Pushpinder Walia: Data curation, Investigation – Experiments, Writing-draft preparation. Yaoyu Fu: Data curation, Investigation – Experiments. Jack Norfleet: Supervision. Steven D. Schwaitzberg: Supervision. Xavier Intes: Supervision. Suvranu De: Supervision, Writing-Reviewing and Editing. Lora Cavuoto: Supervision, Writing-Reviewing and Editing. Anirban Dutta: Conceptualization, Methodology, Writing- Reviewing and Editing.

Funding

The authors gratefully acknowledge the support of this work through the Medical Technology Enterprise Consortium (MTEC) award #W81XWH2090019 (2020-628), and the U.S. Army Futures Command, Combat Capabilities Development Command Soldier Center STTC cooperative research agreement #W912CG-21-2-0001.

References

Aasted, C. M., Yücel, M. A., Cooper, R. J., Dubb, J., Tsuzuki, D., Becerra, L., et al. (2015). Anatomical guidance for functional near-infrared spectroscopy: AtlasViewer tutorial. *Neurophotonics* 2. doi: 10.1117/1.NPh.2.2.020801.

Albert, S. T., Jang, J., Sheahan, H. R., Teunissen, L., Vandevoorde, K., Herzfeld, D. J., et al. (2021). An implicit memory of errors limits human sensorimotor adaptation. *Nat Hum Behav* 5, 920–934. doi: 10.1038/s41562-020-01036-x.

Allen, J. W., Rivas, H., Cocchione, R. N., and Ferzli, G. S. (2003). Intracorporeal Suturing and Knot Tying Broadens the Clinical Applicability of Laparoscopy. *JSLS® : Journal of the Society of Laparoendoscopic Surgeons* 7, 137.

Preprints (www.preprints.org) | NOT PEER-REVIEWED | Posted: 19 April 2022 doi:10.20944/preprints202204.0175.v1

Badre, D. (2008). Cognitive control, hierarchy, and the rostro–caudal organization of the frontal lobes. *Trends in Cognitive Sciences* 12, 193–200. doi: 10.1016/j.tics.2008.02.004.

Badre, D., and D'Esposito, M. (2009a). Is the rostro-caudal axis of the frontal lobe hierarchical? *Nature Reviews Neuroscience* 10, 659–669. doi: 10.1038/nrn2667.

Badre, D., and D'Esposito, M. (2009b). Is the rostro-caudal axis of the frontal lobe hierarchical? *Nature Reviews Neuroscience* 10, 659–669. doi: 10.1038/nrn2667.

Benozzo, D., Camera, G. L., and Genovesio, A. (2021). Slower prefrontal metastable dynamics during deliberation predicts error trials in a distance discrimination task. *Cell Reports* 35. doi: 10.1016/j.celrep.2021.108934.

Birkmeyer, J. D., Finks, J. F., O'Reilly, A., Oerline, M., Carlin, A. M., Nunn, A. R., et al. (2013). Surgical Skill and Complication Rates after Bariatric Surgery. *New England Journal of Medicine* 369, 1434–1442. doi: 10.1056/nejmsa1300625.

Britz, J., Van De Ville, D., and Michel, C. M. (2010). BOLD correlates of EEG topography reveal rapid resting-state network dynamics. *Neuroimage* 52, 1162–1170. doi: 10.1016/j.neuroimage.2010.02.052.

Chang, C.-Y., Hsu, S.-H., Pion-Tonachini, L., and Jung, T.-P. (2020). Evaluation of Artifact Subspace Reconstruction for Automatic Artifact Components Removal in Multi-Channel EEG Recordings. *IEEE Transactions on Biomedical Engineering* 67, 1114–1121. doi: 10.1109/TBME.2019.2930186.

Christensen, A., Giese, M. A., Sultan, F., Mueller, O. M., Goericke, S. L., Ilg, W., et al. (2014). An intact action-perception coupling depends on the integrity of the cerebellum. *J Neurosci* 34, 6707–6716. doi: 10.1523/JNEUROSCI.3276-13.2014.

Christoff, K., and Gabrieli, J. D. E. (2000). The frontopolar cortex and human cognition: Evidence for a rostrocaudal hierarchical organization within the human prefrontal cortex. *Psychobiology* 28, 168–186. doi: 10.3758/BF03331976.

Crick, F. (1984). Function of the thalamic reticular complex: the searchlight hypothesis. *Proc Natl Acad Sci U S A* 81, 4586–4590. doi: 10.1073/pnas.81.14.4586.

Custo, A., Van De Ville, D., Wells, W. M., Tomescu, M. I., Brunet, D., and Michel, C. M. (2017). Electroencephalographic Resting-State Networks: Source Localization of Microstates. *Brain Connect* 7, 671–682. doi: 10.1089/brain.2016.0476.

Debaere, F., Wenderoth, N., Sunaert, S., Van Hecke, P., and Swinnen, S. P. (2004). Cerebellar and premotor function in bimanual coordination: parametric neural responses to spatiotemporal complexity and cycling frequency. *Neuroimage* 21, 1416–1427. doi: 10.1016/j.neuroimage.2003.12.011.

Dehabadi, M., Fernando, B., and Berlingieri, P. (2014). The use of simulation in the acquisition of laparoscopic suturing skills. *International Journal of Surgery* 12, 258–268. doi: 10.1016/J.IJSU.2014.01.022.

Diedrichsen, J., White, O., Newman, D., and Lally, N. (2010). Use-Dependent and Error-Based Learning of Motor Behaviors. *J. Neurosci.* 30, 5159–5166. doi: 10.1523/JNEUROSCI.5406-09.2010.

Ebner, T. J. (2013). "Cerebellum and Internal Models," in *Handbook of the Cerebellum and Cerebellar Disorders* (Springer, Dordrecht), 1279–1295. doi: 10.1007/978-94-007-1333-8_56.

Ericsson, K. A. (2006). "The Influence of Experience and Deliberate Practice on the Development of Superior Expert Performance," in *The Cambridge Handbook of Expertise and Expert Performance* Cambridge Handbooks in Psychology., eds. K. A. Ericsson, N. Charness, P. J. Feltovich, and R. R. Hoffman (Cambridge: Cambridge University Press), 683–704. doi: 10.1017/CBO9780511816796.038.

Fuster, J. M. (2004). Upper processing stages of the perception-action cycle. *Trends Cogn Sci* 8, 143–145. doi: 10.1016/j.tics.2004.02.004.

Gao, Y., Cavuoto, L., Dutta, A., Kruger, U., Yan, P., Nemani, A., et al. (2021a). Decreasing the Surgical Errors by Neurostimulation of Primary Motor Cortex and the Associated Brain Activation via Neuroimaging. *Front Neurosci* 15, 651192. doi: 10.3389/fnins.2021.651192.

Preprints (www.preprints.org) | NOT PEER-REVIEWED | Posted: 19 April 2022 doi:10.20944/preprints202204.0175.v1

Gao, Y., Yan, P., Kruger, U., Cavuoto, L., Schwaitzberg, S., De, S., et al. (2021b). Functional Brain Imaging Reliably Predicts Bimanual Motor Skill Performance in a Standardized Surgical Task. *IEEE Trans Biomed Eng* 68, 2058–2066. doi: 10.1109/TBME.2020.3014299.

Gehring, W. J., and Fencsik, D. E. (2001). Functions of the Medial Frontal Cortex in the Processing of Conflict and Errors. *J Neurosci* 21, 9430–9437. doi: 10.1523/JNEUROSCI.21-23-09430.2001.

Gerraty, R. T., Davidow, J. Y., Wimmer, G. E., Kahn, I., and Shohamy, D. (2014). Transfer of learning relates to intrinsic connectivity between hippocampus, ventromedial prefrontal cortex, and large-scale networks. *J Neurosci* 34, 11297–11303. doi: 10.1523/JNEUROSCI.0185-14.2014.

Grantcharov, T. P., and Funch-Jensen, P. (2009). Can everyone achieve proficiency with the laparoscopic technique? Learning curve patterns in technical skills acquisition. *Am J Surg* 197, 447–449. doi: 10.1016/j.amjsurg.2008.01.024.

Gu, Q. L., Lam, N. H., Wimmer, R. D., Halassa, M. M., and Murray, J. D. (2021). Computational Circuit Mechanisms Underlying Thalamic Control of Attention. doi: 10.1101/2020.09.16.300749.

Hannah, T. C., Turner, D., Kellner, R., Bederson, J., Putrino, D., and Kellner, C. P. (2022). Neuromonitoring Correlates of Expertise Level in Surgical Performers: A Systematic Review. *Front Hum Neurosci* 16, 705238. doi: 10.3389/fnhum.2022.705238.

Heitger, M. H., Ronsse, R., Dhollander, T., Dupont, P., Caeyenberghs, K., and Swinnen, S. P. (2012). Motor learning-induced changes in functional brain connectivity as revealed by means of graph-theoretical network analysis. *NeuroImage* 61, 633–650. doi: 10.1016/j.neuroimage.2012.03.067.

Holroyd, C. B., and Coles, M. G. H. (2002). The neural basis of human error processing: reinforcement learning, dopamine, and the error-related negativity. *Psychol Rev* 109, 679–709. doi: 10.1037/0033-295X.109.4.679.

Hughes, S. W., Lörincz, M., Cope, D. W., Blethyn, K. L., Kékesi, K. A., Parri, H. R., et al. (2004). Synchronized Oscillations at α and θ Frequencies in the Lateral Geniculate Nucleus. *Neuron* 42, 253–268. doi: 10.1016/S0896-6273(04)00191-6.

Ide, J. S., and Li, C. R. (2011). A cerebellar thalamic cortical circuit for error-related cognitive control. *Neuroimage* 54, 455–464. doi: 10.1016/j.neuroimage.2010.07.042.

Jahani, S., Setarehdan, S. K., Boas, D. A., and Yücel, M. A. (2018). Motion artifact detection and correction in functional near-infrared spectroscopy: a new hybrid method based on spline interpolation method and Savitzky-Golay filtering. *Neurophotonics* 5, 015003. doi: 10.1117/1.NPh.5.1.015003.

Keles, H. O., Barbour, R. L., and Omurtag, A. (2016). Hemodynamic correlates of spontaneous neural activity measured by human whole-head resting state EEG+fNIRS. *Neuroimage* 138, 76–87. doi: 10.1016/j.neuroimage.2016.05.058.

Khoe, H. C. H., Low, J. W., Wijerathne, S., Ann, L. S., Salgaonkar, H., Lomanto, D., et al. (2020). Use of prefrontal cortex activity as a measure of learning curve in surgical novices: results of a single blind randomised controlled trial. *Surg Endosc* 34, 5604–5615. doi: 10.1007/s00464-019-07331-7.

Koechlin, E., and Summerfield, C. (2007). An information theoretical approach to prefrontal executive function. *Trends Cogn Sci* 11, 229–235. doi: 10.1016/j.tics.2007.04.005.

Kumar, D., Sinha, N., Dutta, A., and Lahiri, U. (2019). Virtual reality-based balance training system augmented with operant conditioning paradigm. *BioMedical Engineering OnLine* 18, 90. doi: 10.1186/s12938-019-0709-3.

Leff, D. R., Leong, J., Yang, G.-Z., and Darzi, A. W. (2008a). Visuo-spatial ability and fMRI cortical activation in surgery residents. *Am J Surg* 195, 138. doi: 10.1016/j.amjsurg.2007.05.036.

Leff, D. R., Orihuela-Espina, F., Atallah, L., Athanasiou, T., Leong, J. J. H., Darzi, A. W., et al. (2008b). Functional prefrontal reorganization accompanies learning-associated refinements in surgery: a manifold embedding approach. *Comput Aided Surg* 13, 325–339. doi: 10.3109/10929080802531482.

Preprints (www.preprints.org) | NOT PEER-REVIEWED | Posted: 19 April 2022 doi:10.20944/preprints202204.0175.v1

Leff, D. R., Orihuela-Espina, F., Atallah, L., Darzi, A., and Yang, G.-Z. (2007). Functional near infrared spectroscopy in novice and expert surgeons--a manifold embedding approach. *Med Image Comput Comput Assist Interv* 10, 270–277. doi: 10.1007/978-3-540-75759-7_33.

Leff, D. R., Orihuela-Espina, F., Leong, J., Darzi, A., and Yang, G.-Z. (2008c). Modelling dynamic fronto-parietal behaviour during minimally invasive surgery--a Markovian trip distribution approach. *Med Image Comput Comput Assist Interv* 11, 595–602. doi: 10.1007/978-3-540-85990-1_71.

Lehmann, D., Ozaki, H., and Pal, I. (1987). EEG alpha map series: brain micro-states by space-oriented adaptive segmentation. *Electroencephalogr Clin Neurophysiol* 67, 271–288. doi: 10.1016/0013-4694(87)90025-3.

Levy, B. J., and Wagner, A. D. (2011). Cognitive control and right ventrolateral prefrontal cortex: reflexive reorienting, motor inhibition, and action updating. *Ann N Y Acad Sci* 1224, 40–62. doi: 10.1111/j.1749-6632.2011.05958.x.

Li, X., Krol, M. A., Jahani, S., Boas, D. A., Tager-Flusberg, H., and Yücel, M. A. (2020). Brain correlates of motor complexity during observed and executed actions. *Scientific Reports* 10, 10965. doi: 10.1038/s41598-020-67327-5.

Maier, M. E., Ernst, B., and Steinhauser, M. (2019). Error-related pupil dilation is sensitive to the evaluation of different error types. *Biological Psychology* 141, 25–34. doi: 10.1016/j.biopsycho.2018.12.013.

Michel, C. M., and Koenig, T. (2018). EEG microstates as a tool for studying the temporal dynamics of whole-brain neuronal networks: A review. *NeuroImage* 180, 577–593. doi: 10.1016/j.neuroimage.2017.11.062.

Milner, A. D. (2017). How do the two visual streams interact with each other? *Exp Brain Res* 235, 1297–1308. doi: 10.1007/s00221-017-4917-4.

Numssen, O., Bzdok, D., and Hartwigsen, G. (2021). Functional specialization within the inferior parietal lobes across cognitive domains. *eLife* 10, e63591. doi: 10.7554/eLife.63591.

Ohuchida, K., Kenmotsu, H., Yamamoto, A., Sawada, K., Hayami, T., Morooka, K., et al. (2009). The frontal cortex is activated during learning of endoscopic procedures. *Surgical Endoscopy*. doi: 10.1007/s00464-008-0316-z.

PE, R., B, L., NA, L., and E, S. (1980). Supplementary motor area and other cortical areas in organization of voluntary movements in man. *Journal of neurophysiology* 43, 118–136. doi: 10.1152/JN.1980.43.1.118.

Perri, R. L., Berchicci, M., Lucci, G., Spinelli, D., and Di Russo, F. (2016). How the brain prevents a second error in a perceptual decision-making task. *Sci Rep* 6, 32058. doi: 10.1038/srep32058.

Perrin, F., Pernier, J., Bertrand, O., and Echallier, J. F. (1989). Spherical splines for scalp potential and current density mapping. *Electroencephalography and Clinical Neurophysiology* 72, 184–187. doi: 10.1016/0013-4694(89)90180-6.

Pirondini, E., Coscia, M., Minguillon, J., Millán, J. del R., Van De Ville, D., and Micera, S. (2017). EEG topographies provide subject-specific correlates of motor control. *Sci Rep* 7, 13229. doi: 10.1038/s41598-017-13482-1.

Poldrack, R. A., Sabb, F. W., Foerde, K., Tom, S. M., Asarnow, R. F., Bookheimer, S. Y., et al. (2005). The Neural Correlates of Motor Skill Automaticity. *J Neurosci* 25, 5356–5364. doi: 10.1523/JNEUROSCI.3880-04.2005.

Poulsen, A. T., Pedroni, A., Langer, N., and Hansen, L. K. (2018). Microstate EEGlab toolbox: An introductory guide. doi: 10.1101/289850.

Raos, V., and Savaki, H. E. (2017). The Role of the Prefrontal Cortex in Action Perception. *Cerebral Cortex* 27, 4677–4690. doi: 10.1093/CERCOR/BHW261.

Rezaee, Z., Ranjan, S., Solanki, D., Bhattacharya, M., Srivastava, M. V. P., Lahiri, U., et al. (2021). Feasibility of combining functional near-infrared spectroscopy with electroencephalography to identify chronic stroke responders to cerebellar transcranial direct current stimulation-a computational modeling and portable neuroimaging methodological study. *Cerebellum*. doi: 10.1007/s12311-021-01249-4.

Ritter, E. M., and Scott, D. J. (2007). Design of a proficiency-based skills training curriculum for the fundamentals of laparoscopic surgery. *Surg Innov* 14, 107–112. doi: 10.1177/1553350607302329.

Preprints (www.preprints.org) | NOT PEER-REVIEWED | Posted: 19 April 2022 doi:10.20944/preprints202204.0175.v1

Roberts, K. E., Bell, R. L., and Duffy, A. J. (2006). Evolution of surgical skills training. *World Journal of Gastroenterology* 12, 3219–3224. doi: 10.3748/wjg.v12.i20.3219.

Rolls, E. T., Huang, C.-C., Lin, C.-P., Feng, J., and Joliot, M. (2020). Automated anatomical labelling atlas 3. *NeuroImage* 206, 116189. doi: 10.1016/j.neuroimage.2019.116189.

Sedaghat-Nejad, E., and Shadmehr, R. (2021). The cost of correcting for error during sensorimotor adaptation. *Proceedings of the National Academy of Sciences* 118, e2101717118. doi: 10.1073/pnas.2101717118.

Seidler, R. D., Kwak, Y., Fling, B. W., and Bernard, J. A. (2013). Neurocognitive Mechanisms of Error-Based Motor Learning. *Adv Exp Med Biol* 782, 10.1007/978-1-4614-5465–6_3. doi: 10.1007/978-1-4614-5465-6_3.

Shadmehr, R., Smith, M. A., and Krakauer, J. W. (2010). Error correction, sensory prediction, and adaptation in motor control. *Annu. Rev. Neurosci.* 33, 89–108. doi: 10.1146/annurev-neuro-060909-153135.

Sirpal, P., Damseh, R., Peng, K., Nguyen, D. K., and Lesage, F. (2021). Multimodal Autoencoder Predicts fNIRS Resting State From EEG Signals. *Neuroinform*. doi: 10.1007/s12021-021-09538-3.

Skrandies, W. (1990). Global field power and topographic similarity. *Brain Topogr* 3, 137–141. doi: 10.1007/BF01128870.

Sood, M., Besson, P., Muthalib, M., Jindal, U., Perrey, S., Dutta, A., et al. (2016). NIRS-EEG joint imaging during transcranial direct current stimulation: Online parameter estimation with an autoregressive model. *J. Neurosci. Methods* 274, 71–80. doi: 10.1016/j.jneumeth.2016.09.008.

Strangman, G. E., Li, Z., and Zhang, Q. (2013). Depth Sensitivity and Source-Detector Separations for Near Infrared Spectroscopy Based on the Colin27 Brain Template. *PLoS One* 8, e66319. doi: 10.1371/journal.pone.0066319.

Swinnen, S. P., and Wenderoth, N. (2004). Two hands, one brain: cognitive neuroscience of bimanual skill. *Trends Cogn Sci* 8, 18–25. doi: 10.1016/j.tics.2003.10.017.

Tanji, J., Okano, K., and Sato, K. C. (1988). Neuronal activity in cortical motor areas related to ipsilateral, contralateral, and bilateral digit movements of the monkey. *J Neurophysiol* 60, 325–343. doi: 10.1152/jn.1988.60.1.325.

Toner, J., Montero, B. G., and Moran, A. (2015). The Perils of Automaticity. *Review of General Psychology* 19, 431–442. doi: 10.1037/gpr0000054.

Toner, J., and Moran, A. (2021). Exploring the orthogonal relationship between controlled and automated processes in skilled action. *Review of Philosophy and Psychology* 12, 577–593. doi: 10.1007/s13164-020-00505-6.

van Elk, M. (2014). The left inferior parietal lobe represents stored hand-postures for object use and action prediction. *Frontiers in Psychology* 5. Available at: https://www.frontiersin.org/article/10.3389/fpsyg.2014.00333 [Accessed April 16, 2022].

Vetter, P., Flash, T., and Wolpert, D. M. (2002). Planning Movements in a Simple Redundant Task. *Current Biology* 12, 488–491. doi: 10.1016/S0960-9822(02)00715-7.

Villringer, A., Planck, J., Hock, C., Schleinkofer, L., and Dirnagl, U. (1993). Near infrared spectroscopy (NIRS): A new tool to study hemodynamic changes during activation of brain function in human adults. *Neuroscience Letters* 154, 101–104. doi: 10.1016/0304-3940(93)90181-J.

von Lühmann, A., Li, X., Müller, K.-R., Boas, D. A., and Yücel, M. A. (2020). Improved physiological noise regression in fNIRS: A multimodal extension of the General Linear Model using temporally embedded Canonical Correlation Analysis. *NeuroImage* 208, 116472. doi: 10.1016/j.neuroimage.2019.116472.

Walia, P., Fu, Y., Schwaitzberg, S. D., Intes, X., De, S., Cavuoto, L., et al. (2021a). Neuroimaging guided tES to facilitate complex laparoscopic surgical tasks – insights from functional near-infrared spectroscopy. doi: 10.21203/rs.3.rs-730076/v1.

Walia, P., Kumar, K. N., and Dutta, A. (2021b). Neuroimaging Guided Transcranial Electrical Stimulation in Enhancing Surgical Skill Acquisition. Comment on Hung et al. The Efficacy of Transcranial Direct Current Stimulation in

Preprints (www.preprints.org) | NOT PEER-REVIEWED | Posted: 19 April 2022 doi:10.20944/preprints202204.0175.v1

Enhancing Surgical Skill Acquisition: A Preliminary Meta-Analysis of Randomized Controlled Trials. Brain Sci. 2021, 11, 707. *Brain Sciences* 11, 1078. doi: 10.3390/brainsci11081078.

Wanzel, K. R., Anastakis, D. J., McAndrews, M. P., Grober, E. D., Sidhu, R. S., Taylor, K., et al. (2007). Visual-spatial ability and fMRI cortical activation in surgery residents. *Am J Surg* 193, 507–510. doi: 10.1016/j.amjsurg.2006.11.011.

Wessel, J. R. (2012). Error awareness and the error-related negativity: evaluating the first decade of evidence. *Front Hum Neurosci* 6, 88. doi: 10.3389/fnhum.2012.00088.

Wolpert, D. M., Miall, R. C., and Kawato, M. (1998). Internal models in the cerebellum. *Trends Cogn. Sci. (Regul. Ed.)* 2, 338–347.

Preprints (www.preprints.org) | NOT PEER-REVIEWED | Posted: 19 April 2022 doi:10.20944/preprints202204.0175.v1

Supplementary Materials – code for statistical tests in Matlab

```
% SYNTAX:
% [hmrstatsG_cond] = hmrG_t_HRF_contrast2(yAvgSubjs1, yAvgSubjs2, tHRFrange)
%
% UI NAME:
% t-test
%
% DESCRIPTION:
% Performs a t-test between two mean HRF for a single condition across all subjects
%
% INPUTS:
% yAvgSubjs: yAvgSubjs1 for group 1 and yAvgSubjs2 for group 2
% tHRFrange: tHRF range for HRF averaging
%
% OUTPUTS:
% hmrstatsG_cond: Statistical results from the MATLAB ttest (h,p,c,stats) and measurement
list (ml)
%
% USAGE OPTIONS:
% Stats_on_Concentration_Data: [hmrstatsG_base_cond] = hmrG_t_HRF_contrast2(dcAvgSubjs1,
dcAvgSubjs2, tHRFrange)
%
% PARAMETERS:
% tHRFrange: [0, 0]
%
function  [hmrstatsG_cond] = hmrG_t_HRF_contrast2(yAvgSubjs1, yAvgSubjs2, tHRFrange)
hmrstatsG_base_cond = [];
iBlk=1;

nSubj = length(yAvgSubjs1);
for iSubj = 1:nSubj

    yAvg     = yAvgSubjs1{iSubj}(iBlk).GetDataTimeSeries('reshape');
    ncond = size(yAvg,4);

    if iSubj == 1
        tHRF     = yAvgSubjs1{iSubj}(iBlk).GetTime();
        fq = abs(1/(tHRF(1)-tHRF(2)));
        ml    = yAvgSubjs1{iSubj}(iBlk).GetMeasListSrcDetPairs();

        % error check
```

Preprints (www.preprints.org) | NOT PEER-REVIEWED | Posted: 19 April 2022 doi:10.20944/preprints202204.0175.v1


```
        if tHRFrange(1)>max(tHRF) || tHRFrange(2)>max(tHRF) || tHRFrange(1)>=tHRFrange(2)
            warning('tHRF range should be between 0 and tHRF max');
            return
        end
    end

    baseline_yAvg1(iSubj,:,:,:)                                                    =
squeeze(mean(yAvg(1:round(fq*abs(min(tHRF))),:,:,:),1));
    mean_yAvg1(iSubj,:,:,:)      =      squeeze(mean(yAvg(round(fq*(tHRFrange(1)      +
abs(min(tHRF)))):round(fq*(tHRFrange(2) + abs(min(tHRF)))),:,:,:),1));
    mean_yAvg1(iSubj,:,:,:) = mean_yAvg1(iSubj,:,:,:) - baseline_yAvg1(iSubj,:,:,:);
end

nSubj = length(yAvgSubjs2);
for iSubj = 1:nSubj

    yAvg     = yAvgSubjs2{iSubj}(iBlk).GetDataTimeSeries('reshape');
    ncond = size(yAvg,4);

    if iSubj == 1
        tHRF     = yAvgSubjs2{iSubj}(iBlk).GetTime();
        fq = abs(1/(tHRF(1)-tHRF(2)));
        ml    = yAvgSubjs2{iSubj}(iBlk).GetMeasListSrcDetPairs();

        % error check
        if tHRFrange(1)>max(tHRF) || tHRFrange(2)>max(tHRF) || tHRFrange(1)>=tHRFrange(2)
            warning('tHRF range should be between 0 and tHRF max');
            return
        end
    end

    baseline_yAvg2(iSubj,:,:,:)                                                    =
squeeze(mean(yAvg(1:round(fq*abs(min(tHRF))),:,:,:),1));
    mean_yAvg2(iSubj,:,:,:)      =      squeeze(mean(yAvg(round(fq*(tHRFrange(1)      +
abs(min(tHRF)))):round(fq*(tHRFrange(2) + abs(min(tHRF)))),:,:,:),1));
    mean_yAvg2(iSubj,:,:,:) = mean_yAvg2(iSubj,:,:,:) - baseline_yAvg2(iSubj,:,:,:);
end

% get t-stats
for iCond = 1:ncond
    for i = 1:size(yAvg, 2)  % HbO/R/T
        for j = 1:size(yAvg,3) % Channels
```

Preprints (www.preprints.org) | NOT PEER-REVIEWED | Posted: 19 April 2022 doi:10.20944/preprints202204.0175.v1


```
            [h,p,c,stats] = ttest2(mean_yAvg1(:,i,j,iCond),mean_yAvg2(:,i,j,iCond));
            pval(i,j,iCond) = p;
            hval(i,j,iCond) = h;
            cval(i,j,iCond,:) = c;
            tstats{i,j,iCond} = stats;

        end
    end
end

% output
hmrstatsG_cond.pval = pval;
hmrstatsG_cond.hval = hval;
hmrstatsG_cond.cval = cval;
hmrstatsG_cond.tstats = tstats;
hmrstatsG_cond.ml = ml;
hmrstatsG_cond.mean_yAvg1 = mean_yAvg1;
hmrstatsG_cond.mean_yAvg2 = mean_yAvg2;


% fdr_bh() - Executes the Benjamini & Hochberg (1995) and the Benjamini &
%           Yekutieli (2001) procedure for controlling the false discovery
%           rate (FDR) of a family of hypothesis tests. FDR is the expected
%           proportion of rejected hypotheses that are mistakenly rejected
%           (i.e., the null hypothesis is actually true for those tests).
%           FDR is a somewhat less conservative/more powerful method for
%           correcting for multiple comparisons than procedures like Bonferroni
%           correction that provide strong control of the family-wise
%           error rate (i.e., the probability that one or more null
%           hypotheses are mistakenly rejected).
%
%           This function also returns the false coverage-statement rate
%           (FCR)-adjusted selected confidence interval coverage (i.e.,
%           the coverage needed to construct multiple comparison corrected
%           confidence intervals that correspond to the FDR-adjusted p-values).
%
%
% Usage:
%  >> [h, crit_p, adj_ci_cvrg, adj_p]=fdr_bh(pvals,q,method,report);
%
% Required Input:
```

Preprints (www.preprints.org) | NOT PEER-REVIEWED | Posted: 19 April 2022 doi:10.20944/preprints202204.0175.v1


```
%   pvals - A vector or matrix (two dimensions or more) containing the
%           p-value of each individual test in a family of tests.
%
% Optional Inputs:
%   q      - The desired false discovery rate. {default: 0.05}
%   method  - ['pdep' or 'dep'] If 'pdep,' the original Bejnamini & Hochberg
%             FDR procedure is used, which is guaranteed to be accurate if
%             the individual tests are independent or positively dependent
%             (e.g., Gaussian variables that are positively correlated or
%             independent).  If 'dep,' the FDR procedure
%             described in Benjamini & Yekutieli (2001) that is guaranteed
%             to be accurate for any test dependency structure (e.g.,
%             Gaussian variables with any covariance matrix) is used. 'dep'
%             is always appropriate to use but is less powerful than 'pdep.'
%             {default: 'pdep'}
%   report  - ['yes' or 'no'] If 'yes', a brief summary of FDR results are
%             output to the MATLAB command line {default: 'no'}
%
%
% Outputs:
%   h      - A binary vector or matrix of the same size as the input "pvals."
%             If the ith element of h is 1, then the test that produced the
%             ith p-value in pvals is significant (i.e., the null hypothesis
%             of the test is rejected).
%   crit_p  - All uncorrected p-values less than or equal to crit_p are
%             significant (i.e., their null hypotheses are rejected).  If
%             no p-values are significant, crit_p=0.
%   adj_ci_cvrg - The FCR-adjusted BH- or BY-selected
%             confidence interval coverage. For any p-values that
%             are significant after FDR adjustment, this gives you the
%             proportion of coverage (e.g., 0.99) you should use when generating
%             confidence intervals for those parameters. In other words,
%             this allows you to correct your confidence intervals for
%             multiple comparisons. You can NOT obtain confidence intervals
%             for non-significant p-values. The adjusted confidence intervals
%             guarantee that the expected FCR is less than or equal to q
%             if using the appropriate FDR control algorithm for the
%             dependency structure of your data (Benjamini & Yekutieli, 2005).
%             FCR (i.e., false coverage-statement rate) is the proportion
%             of confidence intervals you construct
%             that miss the true value of the parameter. adj_ci=NaN if no
%             p-values are significant after adjustment.
```

Preprints (www.preprints.org) | NOT PEER-REVIEWED | Posted: 19 April 2022 doi:10.20944/preprints202204.0175.v1


```
%   adj_p   - All adjusted p-values less than or equal to q are significant
%             (i.e., their null hypotheses are rejected). Note, adjusted
%             p-values can be greater than 1.
%
%
% References:
%   Benjamini, Y. & Hochberg, Y. (1995) Controlling the false discovery
%     rate: A practical and powerful approach to multiple testing. Journal
%     of the Royal Statistical Society, Series B (Methodological). 57(1),
%     289-300.
%
%   Benjamini, Y. & Yekutieli, D. (2001) The control of the false discovery
%     rate in multiple testing under dependency. The Annals of Statistics.
%     29(4), 1165-1188.
%
%   Benjamini, Y., & Yekutieli, D. (2005). False discovery rate?adjusted
%     multiple confidence intervals for selected parameters. Journal of the
%     American Statistical Association, 100(469), 71?81. doi:10.1198/016214504000001907
%
%
% Example:
%  nullVars=randn(12,15);
%  [~, p_null]=ttest(nullVars); %15 tests where the null hypothesis
%  %is true
%  effectVars=randn(12,5)+1;
%  [~, p_effect]=ttest(effectVars); %5 tests where the null
%  %hypothesis is false
%  [h, crit_p, adj_ci_cvrg, adj_p]=fdr_bh([p_null p_effect],.05,'pdep','yes');
%  data=[nullVars effectVars];
%  fcr_adj_cis=NaN*zeros(2,20); %initialize confidence interval bounds to NaN
%  if ~isnan(adj_ci_cvrg),
%     sigIds=find(h);
%      fcr_adj_cis(:,sigIds)=tCIs(data(:,sigIds),adj_ci_cvrg); % tCIs.m is available on
the
%     %Mathworks File Exchagne
%  end
%
%
% For a review of false discovery rate control and other contemporary
% techniques for correcting for multiple comparisons see:
%
%   Groppe, D.M., Urbach, T.P., & Kutas, M. (2011) Mass univariate analysis
```

Preprints (www.preprints.org) | NOT PEER-REVIEWED | Posted: 19 April 2022 doi:10.20944/preprints202204.0175.v1


```
% of event-related brain potentials/fields I: A critical tutorial review.
% Psychophysiology, 48(12) pp. 1711-1725, DOI: 10.1111/j.1469-8986.2011.01273.x
% http://www.cogsci.ucsd.edu/~dgroppe/PUBLICATIONS/mass_uni_preprint1.pdf
%
%
% For a review of FCR-adjusted confidence intervals (CIs) and other techniques
% for adjusting CIs for multiple comparisons see:
%
%  Groppe, D.M. (in press) Combating the scientific decline effect with
% confidence (intervals). Psychophysiology.
% http://biorxiv.org/content/biorxiv/early/2015/12/10/034074.full.pdf
%
%
% Author:
% David M. Groppe
% Kutaslab
% Dept. of Cognitive Science
% University of California, San Diego
% March 24, 2010

%%%%%%%%%%%%%%%% REVISION LOG %%%%%%%%%%%%%%%%
%
% 5/7/2010-Added FDR adjusted p-values
% 5/14/2013- D.H.J. Poot, Erasmus MC, improved run-time complexity
% 10/2015- Now returns FCR adjusted confidence intervals

function [h, crit_p, adj_ci_cvrg, adj_p]=fdr_bh(pvals,q,method,report)

if nargin<1,
    error('You need to provide a vector or matrix of p-values.');
else
    if ~isempty(find(pvals<0,1)),
        error('Some p-values are less than 0.');
    elseif ~isempty(find(pvals>1,1)),
        error('Some p-values are greater than 1.');
    end
end

if nargin<2,
    q=.05;
end
```

Preprints (www.preprints.org) | NOT PEER-REVIEWED | Posted: 19 April 2022 doi:10.20944/preprints202204.0175.v1


```
if nargin<3,
    method='pdep';
end

if nargin<4,
    report='no';
end

s=size(pvals);
if (length(s)>2) || s(1)>1,
    [p_sorted, sort_ids]=sort(reshape(pvals,1,prod(s)));
else
    %p-values are already a row vector
    [p_sorted, sort_ids]=sort(pvals);
end
[dummy, unsort_ids]=sort(sort_ids); %indexes to return p_sorted to pvals order
m=length(p_sorted); %number of tests

if strcmpi(method,'pdep'),
    %BH procedure for independence or positive dependence
    thresh=(1:m)*q/m;
    wtd_p=m*p_sorted./(1:m);

elseif strcmpi(method,'dep')
    %BH procedure for any dependency structure
    denom=m*sum(1./(1:m));
    thresh=(1:m)*q/denom;
    wtd_p=denom*p_sorted./[1:m];
    %Note, it can produce adjusted p-values greater than 1!
    %compute adjusted p-values
else
    error('Argument ''method'' needs to be ''pdep'' or ''dep''.');
end

if nargout>3,
    %compute adjusted p-values; This can be a bit computationally intensive
    adj_p=zeros(1,m)*NaN;
    [wtd_p_sorted, wtd_p_sindex] = sort( wtd_p );
    nextfill = 1;
    for k = 1 : m
        if wtd_p_sindex(k)>=nextfill
            adj_p(nextfill:wtd_p_sindex(k)) = wtd_p_sorted(k);
```

Preprints (www.preprints.org) | NOT PEER-REVIEWED | Posted: 19 April 2022 doi:10.20944/preprints202204.0175.v1


```
            nextfill = wtd_p_sindex(k)+1;
            if nextfill>m
                break;
            end;
        end;
    end;
    adj_p=reshape(adj_p(unsort_ids),s);
end

rej=p_sorted<=thresh;
max_id=find(rej,1,'last'); %find greatest significant pvalue
if isempty(max_id),
    crit_p=0;
    h=pvals*0;
    adj_ci_cvrg=NaN;
else
    crit_p=p_sorted(max_id);
    h=pvals<=crit_p;
    adj_ci_cvrg=1-thresh(max_id);
end

if strcmpi(report,'yes'),
    n_sig=sum(p_sorted<=crit_p);
    if n_sig==1,
        fprintf('Out of %d tests, %d is significant using a false discovery rate
of %f.\n',m,n_sig,q);
    else
        fprintf('Out of %d tests, %d are significant using a false discovery rate
of %f.\n',m,n_sig,q);
    end
    if strcmpi(method,'pdep'),
        fprintf('FDR/FCR procedure used is guaranteed valid for independent or positively
dependent tests.\n');
    else
        fprintf('FDR/FCR procedure used is guaranteed valid for independent or dependent
tests.\n');
    end
end
```

Preprints (www.preprints.org) | NOT PEER-REVIEWED | Posted: 19 April 2022 doi:10.20944/preprints202204.0175.v1

Preprints (www.preprints.org) | NOT PEER-REVIEWED | Posted: 19 April 2022 doi:10.20944/preprints202204.0175.v1

Supplementary Materials – components in the tCCA latent space

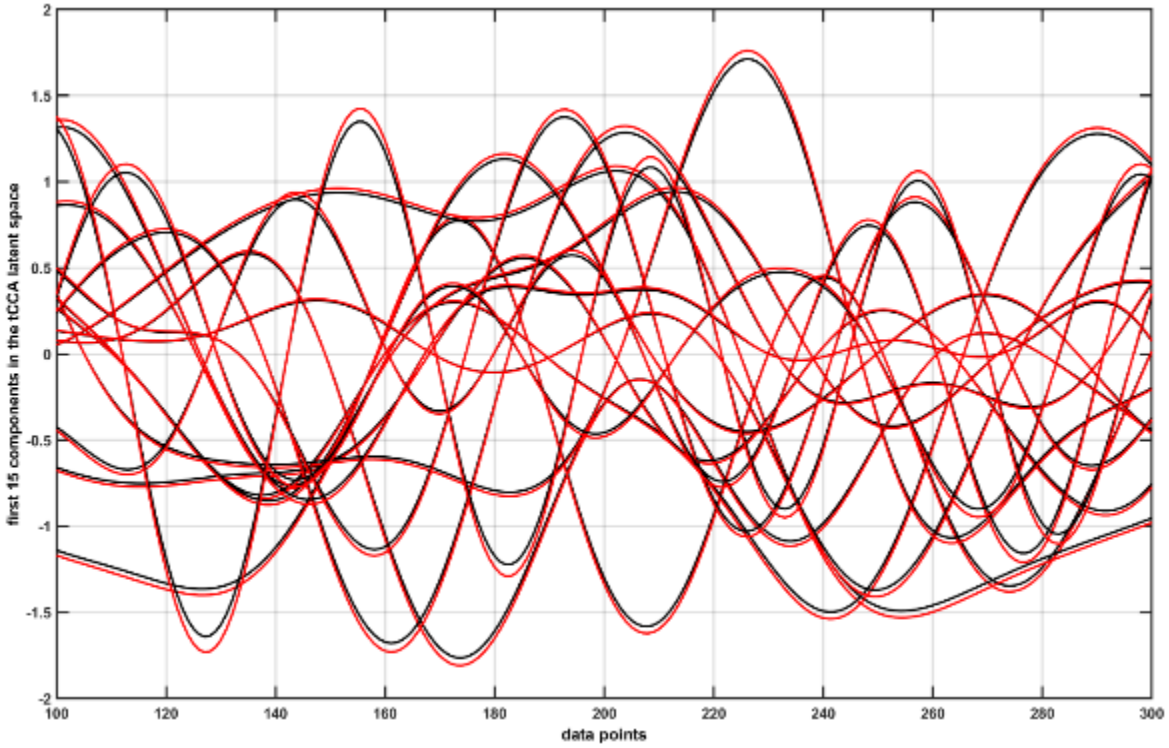

Figure S1: An illustrative plot of the 15 components or sources (greater than the correlation threshold, 0.99) in the tCCA latent space where red are the EEG bandpower (1-40Hz) sources and the black lines are the corresponding HbO sources. The 15 EEG sources were used as the regressors alongwith short-separation nuisance regressors in the GLM to reconstruct the HbO signal.